

On Sedna and the cloud of comets surrounding the Solar System in Milgromian dynamics

R. Paučo and J. Klačka

Faculty of Mathematics, Physics and Informatics, Comenius University in Bratislava, Mlynská dolina, 811 02 Bratislava
e-mail: pauco@fmph.uni.ba.sk

April 23, 2022

ABSTRACT

We reconsider the hypothesis of a vast cometary reservoir surrounding the Solar System - the Oort cloud of comets - within the framework of Milgromian Dynamics (MD or MOND). For this purpose we build a numerical model of the cloud, assuming the theory of modified gravity QUMOND. In modified gravity versions of MD the internal dynamics of a system is influenced by the external gravitational field in which the system is embedded, even when this external field is constant and uniform, a phenomenon dubbed External Field Effect. Adopting popular pair $\nu(x) = [1 - \exp(-x^{1/2})]^{-1}$ for the MD interpolating function and $a_0 = 1.2 \times 10^{-10}$ m s⁻² for the MD acceleration scale as a standard, we have found that the observationally inferred Milgromian cloud of comets is much more radially compact than its Newtonian counterpart. The comets of the Milgromian cloud stay away from the zone where the Galactic tide can torque their orbits significantly. However, this does not need to be an obstacle for injection of the comets into the inner Solar System as the External Field Effect can induce significant change in perihelion distance during one revolution of a comet around the Sun. The efficiency of such injection is further increased by shift of the classical planetary barrier towards the Sun. Adopting constraints on different interpolating function families and revised value of a_0 as found recently by Hees et al. (2016), the aforementioned qualitative results no longer hold and it can be summarized that the Milgromian cloud is very similar to the Newtonian in its overall size, binding energies of comets and hence operation of the Jupiter-Saturn barrier. However, torquing of perihelia due to External Field Effect still play a significant role in the inner parts of the cloud. Consequently Sedna-like orbits and orbits of large semi-major axis Centaurs are easily comprehensible in MD. In MD they both belong to the same population, just in different modes of their evolution. Also one would expect some ‘residual’ population to exist at $a \sim 1000$ au (a is semi-major axis) and $q \gtrsim 100$ au (q is perihelion distance), contrary to the empty space predicted there by Newtonian dynamics.

Key words. comets: general — Galaxy: general, solar neighborhood — gravitation — Oort Cloud

1. Introduction

Our present day theoretical framework of the Universe is general theory of relativity (GTR; with final piece in Einstein 1915), celebrating 100 years of its existence. GTR can be at appropriate limit well substituted with Newtonian gravity as it was constructed to be so, thus at some point GTR was adjusted to observations made at Newton’s era. In order to explain the modern large-scale observations of the Universe with GTR we have to insist on nearly flat non-monotonously accelerating Universe filled with never directly observed ingredients, the so called dark energy (well represented by the cosmological constant Λ) and non-baryonic dark matter (DM, or CDM for cold dark matter), both having very finely tuned properties (e.g., Copeland et al. 2006; Famaey & McGaugh 2013).

Unfortunately Λ CDM model of the Universe is mute in addressing observed dynamical regularities of galaxies, the building blocks of the Universe: baryonic Tully-Fisher relation (Tully & Fisher 1977; McGaugh et al. 2000; McGaugh 2005b), Faber-Jackson relation (Faber & Jackson 1976; Sanders 2010), or the mass discrepancy-acceleration correlation (McGaugh 2004, 2005a). These observations reveal a strong coupling between the baryonic matter and the hypothetical DM. Moreover, they self-consistently point to existence of a special acceleration scale (Famaey & McGaugh 2012).

Observations of our closest cosmic neighbourhood, the Local Group, highly disfavour the standard cosmology based on the particle dark matter (e.g., Kroupa et al. 2010; Kroupa 2012). One of the observations that is hardly to accommodate within Λ CDM, even after baryonic physics is incorporated into the model, is highly anisotropic distribution of the Local Group members - existence of thin coorbiting planes of satellites around Milky Way and M31 (Pawlowski et al. 2012b, 2013, 2014, 2015; Ibata et al. 2013). It has been recently discovered that similarly anisotropic distributions of satellites are possibly common in low redshift Universe ($z < 0.05$; Ibata et al. 2014, 2015). All these issues signal that after 100 years we have *probably* reached the boundaries of GTR and it happened very naturally with the empirical progress. Thus we should put an effort in finding and testing new theory explaining better *the present-day observations*.

The aforementioned galactic phenomenology can be well explained within the framework of Milgromian dynamics (MD or MOND; Milgrom 1983b; Famaey & McGaugh 2012 for a review of 30 years of its evolution). For instance, the thin co-orbiting planes of Local Group satellites can be a by-product of a past close fly-by that Milky Way and M31 have undergone about 7 - 11 Gyr ago (Zhao et al. 2013; Pawlowski et al. 2012a). Thus, we should claim that the new theoretical framework of the Universe we are looking for will explain why everything happens as if galaxies are Milgromian and not Newtonian objects.

The current status of MD is quite analogous to Newton's gravitational law, explaining the Kepler laws of planetary motion, in the Newton's era: MD has strong predictive power although its parent (generally-covariant) theory is still absent (Famaey & McGaugh 2012). MD proposes modification of dynamics that is most apparent in low-acceleration regions of astrophysical systems. In MD a test particle in a point mass gravitational field accelerates towards the point mass with magnitude $(g^N a_0)^{1/2}$ if $g^N \ll a_0$, where g^N is expected Newtonian gravitational field and a_0 is a constant with units of acceleration. The constant $a_0 \sim 10^{-10} \text{ m s}^{-2}$ plays role of a moderator and vice-versa when $g^N \gg a_0$ the classical limit is recovered. However, MD also states (at least when considered as modified gravity) that internal gravitational dynamics of a system is influenced by existence of a constant external gravitational field¹ in which the system is embedded (Milgrom 1983b). In MD external gravity does not decouple from internal dynamics as it does in the Newtonian dynamics; the strong equivalence principle is apparently broken. This so called external field effect (EFE) can attenuate or erase MD effects in the presence of external field of magnitude larger than a_0 even when internal accelerations are well below a_0 , see § 2.3.

Many of new comets entering the inner Solar System can be good probes of modified dynamics as we expect them to originate at large heliocentric distances where the Sun-comet acceleration is very small². When astronomers observing motion of new comets entering the inner Solar System interpret these observations in the framework of Newtonian dynamics (Newtonian astronomers) they end up with the idea of a vast reservoir (radius $\sim 100 \text{ kau}$) of bodies, the Oort cloud (OC; Öpik 1932; Oort 1950), from which are the comets steadily replenished. In the language of the Newtonian orbital elements they do so because they find: (1) a sharp peak in the distribution of the original (i.e., before entering the planetary zone) reciprocal semi-major axes $0 < 1/a_{orig} \lesssim 10^{-4}$ (i.e., orbital energies), and, (2) isotropically distributed perihelia directions. We reserve the terms 'near-parabolic comet' and 'Oort-spike comet' for a comet with semi-major axis greater than 10 kau and perihelion distance between 0 and $\sim 8 \text{ au}$ (i.e., to be observable), as derived by a Newtonian astronomer.

In this paper we investigate change in the view about the Solar System cometary reservoir when the Newtonian dynamics is substituted with Milgromian. We consider exclusively quasi-linear formulation of MD (QUMOND; Milgrom 2010), the classical modified gravity theory constructed in the spirit of MOND (Milgrom 1983b). We stress that the comet is observable only in the deep Newtonian regime where gravity is much larger than the MD threshold value a_0 . The basic structure of the 'cloud' in MD can be thus probed by tracing the motion of the Oort-spike comets back in time, with the actual observations (positions and velocities) serving as the initial conditions. Extending our mainly qualitative analysis into quantitative one presents a profound test of MD.

In the rest of § 1 we briefly review the classical picture of the cometary reservoir. In § 2 we introduce quasi-linear formulation of MD (QUMOND) and the numerical procedure of 'how to move things' in QUMOND. § 3 presents various models of the Solar System nested in the local Galactic environment considered in this paper. The crude picture of the Milgro-

mian OC (MOC) is presented in § 4. In § 5 we examine past QUMOND trajectories of 31 observed near-parabolic comets. In § 6 torquing due to EFE is investigated. Constraints on MD interpolating function families as found recently by Hees et al. (2016) are taken into account in § 7. We conclude and discuss our results in § 8.

1.1. Classical Oort cloud

We refer to the OC whose existence, size and structure are concluded by a Newtonian astronomer as 'the classical OC'.

The standard picture is that the OC with radius of several tens of kau is a natural product of an interplay between scattering of planetesimals by the giant planets - inflating bodies semi-major axes - and tidal torquing by the Galaxy and random passing stars - lifting bodies perihelia out of the planetary zone (Duncan et al. 1987; Dones et al. 2004). Vice-versa reinjection of these bodies into the inner Solar System is moderated by the same dynamical agents (Heisler & Tremaine 1986; Kaib & Quinn 2009). The pivotal role of the Galactic tide, in both enriching and eroding the OC, was fully recognized after the paper of Heisler & Tremaine (1986). Their simplified analytical theory of the Galactic disk tide considering only its vertical component (if we assume that the Galactic equatorial plane is 'horizontal'), as the radial components are nearly an order of magnitude weaker, reveals that effect of the tides is analogous to the effect of the planets on comets of shorter periods - causing the Lydov-Kozai cycles. The vertical component of the comet's orbital angular momentum is conserved and comets follow closed trajectories in $q-\omega$ plane (q is the perihelion distance and ω is the argument of perihelion). Thus, q can be 'traded' for Galactic inclination back and forth while ω librates. As the component of the tidal force that brings comets into visibility is $\sim \sin(2b_G)$, where b_G is galactic latitude of the line of apsides³, a comet experiences the most rapid changes of q per orbit when $b_G = \pm\pi/4$, while when $b_G = 0$ or $b_G = \pm\pi/2$ the changes in perihelion distance are nil (Torbett 1986). Using a sample of long periodic comets (LPCs), with periods larger than 10 000 yrs and accurately known original orbits, Delsemme (1987) also noted these features observationally in the distribution of b_G among the sample comets, confirming the significance of the Galactic tide.

Comets with $q < 15 \text{ au}$ are usually considered lost from the OC, to either interstellar region or a more tightly bound orbit, due to planetary perturbations (phenomenon also called Jupiter-Saturn barrier). The planetary 'kick' they receive is typically much larger than the width of the Oort spike. Thus to be observable a comet has to decrease its perihelia at least by $\sim 10 \text{ au}$ during the revolution preceding its possible discovery from the zone where planets have minor effect down to the observability zone (typically less than 5 au from the Sun). Only the comets with $a > 20 - 30 \text{ kau}$ (defining outer OC; a is the semi-major axis) are experiencing large enough tidal torque to cause such large decrease in q in one revolution (e.g., Dones et al. 2004; Rickman 2014). But, there are many observed Oort spike comets with much smaller semi-major axes (Dybczyński & Królikowska 2011, hereafter DK11). The concept of the Jupiter-Saturn barrier should be actually revised as about 15 per cent of the near-parabolic comets can migrate through it without any significant orbital change (DK11; Dybczyński & Królikowska 2015).

³ angle between the line of apsides and the Galactic plane, if for simplicity the Sun rests in the Galactic plane

¹ In spatially varying gravitational field we have, in addition, the standard tidal effects.

² But note that EFE always attenuates classical MD effects, see § 2.3 for discussion.

Kaib & Quinn (2009) demonstrated importance of a special dynamical pathway capable to deliver inner OC bodies (initial $a < 20$ kau, often even < 10 kau) into the observable orbits - but at first into the outer OC region $a > 20$ kau - by a cooperation between the planetary perturbations and the Galactic tide. According to Kaib & Quinn (2009) the new comets entering the inner Solar System could originate in both, the inner, and also the outer OC, with nearly equal probability.

Passing Galactic-field stars, although their implied injection rate is 1.5 - 2 times smaller than that of the Galactic tide⁴ (Heisler & Tremaine 1986), have its own important role - they keep the OC isotropic. The trajectories with course - the inner Solar System - would be quickly depleted if there were no passing stars. Synergy between the Galactic tide and the passing stars ensures almost steady flow of new comets into the inner Solar System (Rickman et al. 2008). Thus all the mentioned dynamical agents are important in the delivering process.

1.2. Puzzles

Here we briefly review some of the persistent puzzles challenging the classical OC theory.

Simulations of the OC formation indicate that only 1 - 3 % of all bodies scattered by the giant planets are trapped to the present day outer OC orbits (or $\sim 5\%$ into the whole cloud; Dones et al. 2004; Kaib et al. 2011). Such low trapping efficiency leads to some inconsistencies in the standard theory, if we presume that the outer OC is the source of the observed LPCs. Specifically, the primordial protoplanetary disk of planetesimals of the total mass $70 - 300 M_{\oplus}$ is required to explain the observed LPC flux near Earth. Such massive disk is at odds with the giant planets formation theory, leading to their excessive migration and/or formation of additional giant planets (Dones et al. 2004 and references therein). Disk of no more than $50 M_{\oplus}$ is in demand (Morbidelli et al. 2007).

As a possible solution of this problem could serve the existence of the mentioned special dynamical pathway described in Kaib & Quinn (2009), because the trapping efficiency of the inner OC can be an order of magnitude larger than that in the outer OC if the OC formation began in an open cluster (Kaib & Quinn 2008). Anyway, the Sun was more probably born in an embedded cluster (Lada & Lada 2003) encased in interstellar gas and dust. The sketched simple solution could be problematic in the presence of vast amount of gas as in the embedded cluster environment. Aerodynamic gas drag on planetesimals prevents kilometre-sized bodies from entering the cloud and in the most extreme case this first stage of the Solar System evolution did not make any contribution to the cloud (Brasser et al. 2007).

Another outstanding puzzle concerns the observed population ratio between the OC and the scattered disk⁵ (SD). Observations suggest this ratio lies between 100 and 1000 but simulations, that produce these two reservoirs simultaneously, yield the value of the order of 10 (Duncan & Levison 1997; Levison et al. 2008; Kaib & Quinn 2009). The populations are inferred from the observed fluxes of new LPCs and Jupiter-family comets (JFCs), brighter than some reference total magnitude. However, the population ratio estimated in the simulations of the OC and SD formation refers to objects bigger than a given size. Account-

ing for the fact that ‘an LPC is smaller than a JFC with the same total absolute magnitude’, Brasser & Morbidelli (2013) arrive at the discrepancy of the factor of ‘only’ 4.

As early as the first numerical simulations of the OC formation were performed, it was recognized that only bodies with semi-major axes a beyond ~ 2000 au could have their perihelia torqued out of the planetary zone into the OC (Duncan et al. 1987). Bodies with smaller a would have their perihelia still settled near planets. The observed orbital distribution of trans-Neptunian objects (TNOs) have largely agreed with this result. Anyway, two striking exceptions were found - the orbit of Sedna (Brown et al. 2004) and 2012 VP₁₁₃ (Trujillo & Sheppard 2014). With perihelia (q) of 76 and 80 au respectively, these objects do not interact with planets anymore, yet their large semi-major axes of ~ 500 and ~ 250 respectively, point to strong planetary perturbations in the past. Although their semi-major axes are larger than most TNOs, they are still too small to be significantly perturbed by the current local Galactic tide. Thus, these orbits remain unexplained by any known dynamical process in the Solar System (Morbidelli & Levison 2004). Interesting solution of this problem was offered by Kaib et al. (2011), namely, radial migration of the Sun (Sellwood & Binney 2002), which was not accounted properly in any past study. Simulation of Kaib et al. (2011) began with formation of the Galaxy in a large N-body + smooth-particle-hydrodynamics simulation where solar analogues were identified. Then the OC formation around these stars (often substantial radial migrants) were followed under influence of the four giant planets, the Galaxy and randomly passing stars, leading to the conclusion that Sedna can be the classical OC body. Unfortunately, enhanced tidal field due to the Sun’s radial migration (inward with respect to its current position, if we are looking back in time) enhances also erosion of the outer OC, and thus deepens the primordial disk mass problem (Kaib et al. 2011).

1.3. Basics of MOND

According to MOND⁶ algorithm (Milgrom 1983b), the true gravitational acceleration in spherically symmetric systems has to be calculated as:

$$\mathbf{g} = \nu(g^N/a_0) \mathbf{g}^N, \quad (1)$$

where $a_0 \approx 10^{-10} \text{ m s}^{-2} \sim c H_0 \sim c \Lambda^{1/2}$ is the transition acceleration, c is the speed of light, H_0 is the Hubble constant, Λ is the cosmological constant, \mathbf{g}^N is the expected Newtonian acceleration, $|\mathbf{g}^N| \equiv g^N$, and $\nu(\beta)$ is an interpolating function reflecting underlying general theory with properties $\nu(\beta) \rightarrow 1$ for $\beta \gg 1$ and $\nu(\beta) \rightarrow \beta^{-1/2}$ for $\beta \ll 1$. Eq. (1) implies that

$$|\mathbf{g}| \equiv g = (g^N a_0)^{1/2} \Leftrightarrow g^N \ll a_0, \quad (2)$$

and thus it yields exactly the well known scaling relations (McGaugh et al. 2000; Faber & Jackson 1976; Milgrom 1983a). Basics of MOND in Eq. (1) can be equivalently written in the form

$$\mu(g/a_0) \mathbf{g} = \mathbf{g}^N, \quad (3)$$

where $\mu(\alpha) = 1/\nu(\beta)$, $\beta = \alpha \mu(\alpha)$, satisfies $\mu(\alpha) \rightarrow 1$ for $\alpha \gg 1$ and $\mu(\alpha) \rightarrow \alpha$ for $\alpha \ll 1$. Eq. (2), the backbone of MOND/MD,

⁴ If we do not consider very close encounters (which can occur because the process is stochastic) occurring on very large time scales, probably leading to comet showers (Hills 1981).

⁵ It is believed that the scattered disk is the source region of the Jupiter-family comets (Duncan & Levison 1997).

⁶ From now on, when we write ‘MOND’ we mean the 1983 Milgrom’s formulation (Milgrom 1983b), the simple formula in Eq. (1). When we write ‘Milgromian dynamics (MD)’ we mean general theory, like in Bekenstein & Milgrom (1984) on the classical level or in Bekenstein (2004) on the Lorentz-covariant level.

is equivalent to state that: (i) equations of motion are invariant under transformation $(t, \mathbf{r}) \rightarrow (\lambda t, \lambda \mathbf{r})$, $\lambda \in \mathbb{R}$ (Milgrom 2009c), or (ii) gravitational field is enhanced by anti-screening of ordinary masses in some gravitationally polarizable medium characterized by ‘gravitational permittivity’ equal to g/a_0 (Blanchet & Le Tiec 2008, 2009; Blanchet & Bernard 2014). Eventually, MOND can be related to quantum-mechanical processes in the vacuum (Milgrom 1999). Another interesting theory taking ‘the best of both worlds’ of MD and Λ CDM is the recent DM superfluid model (Berezhiani & Khoury 2015a,b).

As MD has higher predictive power in galaxies than Λ CDM model, though its parent (generally-covariant) theory is still missing, and as most of the classical OC lies in MD acceleration regime, modulated by the external field of the Galaxy $\sim 2a_0$, it is demanding to investigate the motion of the Oort spike comets as it is prescribed by MD. Science is mainly about formulating and testing hypotheses. Possible inevitable tension between the theory and observations could be a disproof of some formulations of MD, incorporating Eq. (2).

Maybe application of the non-standard physics does not yield inconsistencies between the OC formation / OC bodies injection models, calibrated by the observed LPC flux, and those of giant planets formation, calibrated by the appearance of the outer planets region.

2. Milgromian dynamics

The simple formula of Eq. (1), considered as modified gravity⁷, cannot be regarded as a universal theory applicable to any self-gravitating system of interest, e.g., for not obeying conservation laws out of highly symmetric problems (Famaey & McGaugh 2012). Anyway, it was recognised, as soon as in Bekenstein & Milgrom (1984) at the classical level and in Bekenstein (2004) at the Lorentz-covariant level, that construction of a universal theory, reproducing Eq. (1) in the special case of the static weak field limit and spherical symmetry, is possible.

2.1. Quasi-linear formulation of MD

Several Lorentz covariant theories of MD has been devised in recent years (e.g., Bekenstein 2004; Sanders 2005; Zlosnik et al. 2007; Milgrom 2009a) reproducing Eq. (1) in the static weak field limit and spherical symmetry, differing from each other outside of it (Zhao & Famaey 2010). At the classical level these generally transform to one of the two types of modified Poisson equation (Bekenstein & Milgrom 1984; Milgrom 2010). Both classical theories are derived from action, thus enjoying the standard conservation laws. The one from Milgrom (2010), dubbed QUMOND for quasi-linear formulation of MD, can be considered as especially attractive for its computational friendliness.

In QUMOND the field equation determining MD potential, Φ , reads

$$\nabla \cdot (\nabla \Phi) = \nabla \cdot \left[\nu(|\nabla \phi^N|/a_0) \nabla \phi^N \right], \quad (4)$$

where ϕ^N is the Newtonian potential fulfilling $\nabla \cdot (\nabla \phi^N) = 4\pi G \varrho_b$, ϱ_b is baryonic mass density. QUMOND comes from

⁷ Eqs. (1) and (3) can be equivalently considered as modified inertia and the whole theory can be build around modifying the kinetic part of the classical action (Milgrom 1994, 2011). We do not consider modified inertia theories in this paper. Note that these are generically non-local theories (Milgrom 1994).

modifying only the gravitational part of the classical action hence the equation of motion stays the same

$$\mathbf{g} = -\nabla \Phi. \quad (5)$$

Let us define the so called ‘phantom matter density’ (PMD)

$$\varrho_{ph} = \frac{\nabla \cdot [\tilde{\nu}(|\nabla \phi^N|/a_0) \nabla \phi^N]}{4\pi G}, \quad (6)$$

$\tilde{\nu}(\beta) \equiv \nu(\beta) - 1$. Eq. (6) does not represent any real physical quantity, particle, nor field. PMD is only a mathematical object allowing us to take advantage of the mentioned QUMOND formulation of MD and write the equations in our intuitive Newtonian sense with ‘dark matter’. With aid of Eq. (6) can be the MD potential Φ written as a sum

$$\Phi = \phi^N + \phi_{ph}, \quad (7)$$

where the phantom potential ϕ_{ph} fulfils normal Poisson equation

$$\nabla \cdot (\nabla \phi_{ph}) = 4\pi G \varrho_{ph}. \quad (8)$$

Once the Newtonian potential is specified PMD can be found and hence the motion in MD can be traced.

Widely used family of $\tilde{\nu}(\beta)$ functions, corresponding to the special behaviour of $\nu(\beta)$ in Eq. (1), is:

$$\tilde{\nu}_n(\beta) = \left[\frac{1 + (1 + 4\beta^{-n})^{1/2}}{2} \right]^{1/n} - 1, \quad (9)$$

see, e.g., Famaey & McGaugh (2012). It is well known that the simple $n = 1$ function (Famaey & Binney 2005) reproduces well the rotation curves of the most spiral galaxies, e.g., Gentile et al. (2011). However, this function is because of its rather gradual transition to the Newtonian regime excluded by Solar System tests, e.g., Sereno & Jetzer (2006), Blanchet & Novak (2011). It is possible to construct interpolating function with more rapid transition to the Newtonian regime (less impact on the Solar System) and in the same time very similar to the simple interpolating function on the galactic scales where accelerations are $\sim a_0$ (see Fig. 19 in Famaey & McGaugh 2012). The one of this kind is McGaugh (2008):

$$\tilde{\nu}(\beta) = \left(1 - e^{-\beta^{1/2}} \right)^{-1} - 1. \quad (10)$$

We use this function, if not stated otherwise, throughout the paper, together with the standard value $a_0 = 1.2 \times 10^{-10} \text{ m s}^{-2} = 3700 \text{ km}^2 \text{ s}^{-2} \text{ kpc}^{-1}$ (Begeman et al. 1991; Gentile et al. 2011; Famaey & McGaugh 2012).

MD greatly reduces missing mass in galaxy clusters but leaves consistent mass discrepancy of factor of about 2 (e.g., Sanders 2003, see also Famaey & McGaugh 2012). This fact is frequently used as a reason to refute completely any consideration of MD⁸. There is a suggestion to avoid the remaining discrepancies with variation of a_0 , and that a_0 is larger in clusters than it is in galaxies (e.g., Zhao & Famaey 2012; Khoury 2015). We do not develop such idea in this paper. In MD the remaining missing mass does not need to be non-baryonic. Instructed by the history and motivated by the ‘missing baryons

⁸ The short argumentation of MD sceptics often goes as ‘the Bullet cluster’. One should bear in mind that in MD theories the mass discrepancies are uniquely predicted by the distribution of baryons but do not need to follow the distribution of baryons exactly.

problem⁹ it is completely possible that we still do not know the whole baryonic budget of the galaxy clusters. The recent discovery of more than a thousand ultra-diffuse galaxy-like objects in the Coma cluster (Koda et al. 2015) further promotes this suggestion (Milgrom 2015).

2.2. Solving for the Milgromian potential of the Galaxy on a grid

One can convert known baryonic matter distribution to QUMOND potential and hence the real acceleration. But in general this has to be done numerically. According to the scheme sketched in Eqs. (5) - (8) we have to at first know the Newtonian potential $\phi^N(\mathbf{r})$, thus we have to solve the Poisson equation $\Delta\phi^N(\mathbf{r}) = 4\pi G\rho_b(\mathbf{r})$, where the baryonic mass density $\rho_b(\mathbf{r})$ is specified by the adopted model of the Galaxy, see § 3.1. For this purpose we employ fast Poisson solver on a cartesian grid with the boundary condition corresponding to a point mass, $\phi^N(r) = -GM_b/r$, on the last grid point, where r is the center of mass distance of the baryonic mass density grid and M_b is the total baryonic mass.

For a given Newtonian potential ϕ^N discretized on a cartesian grid (x, y, z) of step h , the discretized version of Eq. (6) is given on a grid point (i, j, k) by:

$$\rho_{ph}^{i,j,k} = \frac{1}{4\pi Gh^2} \left[\begin{aligned} &(\phi_{i+1,j,k}^N - \phi_{i,j,k}^N)\tilde{v}_{B_x} \\ &- (\phi_{i,j,k}^N - \phi_{i-1,j,k}^N)\tilde{v}_{A_x} \\ &+ (\phi_{i,j+1,k}^N - \phi_{i,j,k}^N)\tilde{v}_{B_y} \\ &- (\phi_{i,j,k}^N - \phi_{i,j-1,k}^N)\tilde{v}_{A_y} \\ &+ (\phi_{i,j,k+1}^N - \phi_{i,j,k}^N)\tilde{v}_{B_z} \\ &- (\phi_{i,j,k}^N - \phi_{i,j,k-1}^N)\tilde{v}_{A_z} \end{aligned} \right], \quad (11)$$

where \tilde{v} function is evaluated in a particular midpoint, e.g., \tilde{v}_{B_x} is evaluated in $(i + 1/2, j, k)$, \tilde{v}_{A_x} in $(i, j - 1/2, k)$, and so on, half a cell from (i, j, k) in each of the three orthogonal directions, see, e.g., Famaey & McGaugh (2012); Lüghausen et al. (2013, 2014, 2015) for illustration. The gradient of ϕ^N in \tilde{v}_{B_x} ($|\nabla\phi^N|/a_0$) is approximated by $\nabla\phi^N = (4\phi_{i+1,j,k}^N - 4\phi_{i,j,k}^N, \phi_{i+1,j+1,k}^N - \phi_{i+1,j-1,k}^N + \phi_{i,j+1,k}^N - \phi_{i,j-1,k}^N, \phi_{i,j,k+1}^N - \phi_{i,j,k-1}^N + \phi_{i+1,j,k+1}^N - \phi_{i+1,j,k-1}^N)/(4h)$, and so forth.

Finally, knowing PMD we can solve for the effective Milgromian potential $\Phi(\mathbf{r})$ in $\Delta\Phi(\mathbf{r}) = 4\pi G[\rho_b(\mathbf{r}) + \rho_{ph}(\mathbf{r})]$ on the same grid. As the boundary condition,

$$\Phi(r) = (GM_b a_0)^{1/2} \ln(r), \quad (12)$$

where r is the center of mass distance of the ‘mass density’ grid and M_b is the total baryonic mass, is assumed on the last grid point, in accordance with Eq. (1). In the whole procedure of obtaining Φ we assume that the Galaxy is isolated from external gravitational fields¹⁰, see § 2.3 for discussion on EFE. This is a good approximation until the internal gravity becomes comparable with the external field generated by the large scale structure

⁹ ≥ 50 per cent of the baryons constrained by the observations of the cosmic microwave background are hidden in some undetected form. Only a small fraction of these hidden baryons would be necessary to account for the mass discrepancy in the galaxy clusters (Famaey & McGaugh 2012).

¹⁰ To avoid confusion, we are treating the Galaxy as being isolated but we consider the Solar System embedded in the field of the Galaxy.

which is of the order of $a_0/100$ (Famaey et al. 2007). At the position of the Sun the internal gravity is $\sim a_0$.

2.3. External field effect

It is a special feature of MD as modified gravity that its formulation breaks the strong equivalence principle (Milgrom 1986b).

Let us have a system s resting in the gravitational field of a larger system S . Say that S generates gravitational acceleration $\mathbf{g}_e = -\nabla\Phi_e$ within s . We assume that gravitational field acting on a body within s , $\mathbf{g} = -\nabla\Phi$, can be separated into internal $\mathbf{g}_i = -\nabla\Phi_i$ ($|\mathbf{g}_i| \equiv g_i$) and external $\mathbf{g}_e = -\nabla\Phi_e$ ($|\mathbf{g}_e| \equiv g_e$) part. Substituting $\nabla\phi^N = \nabla\phi_i^N + \nabla\phi_e^N = -\mathbf{g}_i^N - \mathbf{g}_e^N$ into Eq. (4), where \mathbf{g}_i^N ($|\mathbf{g}_i^N| \equiv g_i^N$) and \mathbf{g}_e^N ($|\mathbf{g}_e^N| \equiv g_e^N$) are internal and external Newtonian gravitational accelerations, gives, after removing divergences, dropping the curl-field and considering only directions in the plane perpendicular to the external field (Angus et al. 2014):

$$\mathbf{g}_i = \nu \left(\frac{\sqrt{(g_i^N)^2 + (g_e^N)^2}}{a_0} \right) \mathbf{g}_i^N, \quad (13)$$

where we have further assumed $\mathbf{g}_e = \nu(g_e^N/a_0)\mathbf{g}_e^N$. The internal gravity in s depends not only on internal gravitational sources (in our case - the Sun) but also on the strength of the external field at the position of s (in our case - the local strength of the Galactic gravitational field), even when the external field is considered to be constant within s .

This effect should not be confused with tidal forces arising from the non-uniformity of the external gravitational field across the system s . A person in the (arbitrarily small) falling elevator in s can find out existence and properties of the external gravitational field through its influence on the internal dynamics. Say g_e^N is constant, if $g_i^N < a_0 \ll g_e^N$ in Eq. (13) the system s behaves purely as Newton said, with no sign of the modified dynamics as $\nu(g_e^N/a_0)$ tends to 1 then, similarly as in the case $g_i^N \gg a_0$. The opposite deep-MD regime applies when $g_e^N < g_i^N \ll a_0$. The standard MD effects are observed only when both internal and external gravity are sufficiently small ($\lesssim a_0$), and moreover the external field does not dominate over the internal one. Eventually if the hierarchy goes as $g_i^N < g_e^N \sim a_0$ the dynamics is Newtonian with rescaled gravitational constant $G/\mu(g_e/a_0) = \nu(g_e^N/a_0)G$, where G is the Newtonian gravitational constant. Moreover, the dynamics is anisotropic with dilatation along the direction of the external field¹¹.

The external field of the Galaxy, \mathbf{g}_e , thus has to be carefully taken into account beyond its tidal effects when modelling MOC. We use the constant value $g_e = V_0^2/R_0 = 240^2 \text{ km}^2 \text{ s}^{-2}/(8.3 \text{ kpc}) \doteq 1.87 a_0$, where V_0 is circular speed of the Sun at R_0 and R_0 is distance between the Sun and the Galactic center (GC), throughout the paper. Compare the values of V_0 and R_0 with, e.g., those given by Schönrich (2012). We take the Newtonian value g_e^N as a solution of

$$g_e = \nu(g_e^N/a_0)g_e^N. \quad (14)$$

Eq. (14) is known to be a good approximation at the position of the Sun (Brada & Milgrom 1995) (the Galaxy can be well modelled as made of bulge plus exponential disks).

Note that the Galactic tide is modelled as separate effect, see § 3.1.3 for details.

¹¹ This is not seen in approximative Eq. (13), but see § 4 where more rigorous approach is applied and anisotropic dynamics is emerging.

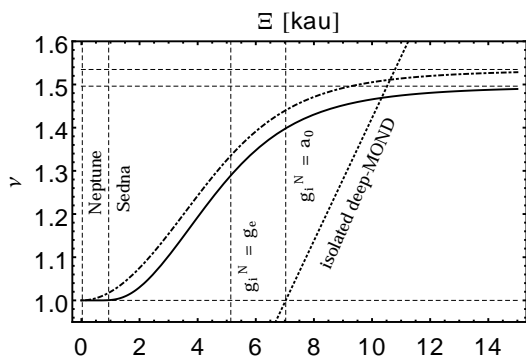


Fig. 1. Interpolating functions $\nu(\beta) = [1 + (1 + 4\beta^{-1})^{1/2}]/2$ (dot-dashed line) and $\nu(\beta) = [1 - \exp(-\beta^{1/2})]^{-1}$ (solid line) as functions of heliocentric distance Ξ . $\beta \equiv g_N/a_0$ is approximated with $[(g_e^N)^2 + (GM_\odot/\Xi^2)^2]^{1/2}/a_0$, i.e. vectors of external and internal Newtonian gravity are assumed to be perpendicular to each other for simplicity. The two topmost horizontal dashed lines are the values ν -functions asymptote to under the condition $\Xi \rightarrow \infty$ (then $g_N \rightarrow g_e^N$), the downmost $\nu = 1$ marks the Newtonian limit. Vertical dashed lines from left to right mark aphelia of Neptune and Sedna and the distances where $GM_\odot/\Xi^2 = g_e = 1.9a_0$ and $GM_\odot/\Xi^2 = a_0$. Dotted line is $\beta^{-1/2} = [(GM_\odot/\Xi^2)/a_0]^{-1/2}$, the deep-MOND limit of $\nu(\beta)$ in the case of no external field.

To better visualise gravity boosting effect of MD and also importance of EFE on the Solar System scales we plot ν interpolating function as a function of heliocentric distance Ξ in Fig. 1. The simple $\nu(\beta) = [1 + (1 + 4\beta^{-1})^{1/2}]/2$ and the exponential $\nu(\beta) = [1 - \exp(-\beta^{1/2})]^{-1}$ interpolating functions are depicted. $\beta \equiv g_N/a_0$ is approximated with $[(g_e^N)^2 + (GM_\odot/\Xi^2)^2]^{1/2}/a_0$, i.e. vectors of external and internal Newtonian gravitational acceleration are assumed to be perpendicular to each other for simplicity. Characteristic distance scale (MD transition scale) is $\sim \sqrt{GM_\odot/a_0} \approx 7$ kau. Due to action of EFE $\nu(\beta)$ does not diverge with $\Xi \rightarrow \infty$ but asymptotes to the constant value $\nu(g_e^N/a_0)$.

EFE is important even in the high-acceleration regime where the gravity boosting effect of MD is very weak. It was shown that at $\Xi \ll \sqrt{GM_\odot/a_0}$, what is well fulfilled in the planetary region, EFE manifests dominantly through an anomalous quadrupolar correction to the Newtonian potential increasing with heliocentric distance Ξ (Milgrom 2009b; Blanchet & Novak 2011). This dynamical effect is thus analogous to that of a massive body, say planet, hidden at large heliocentric distance lying in the direction to GC, \mathbf{g}_e/g_e , (Hogg et al. 1991; Iorio 2010b). As the external field \mathbf{g}_e rotates with period ~ 210 Myr this corresponds to unfeasible configuration in Newtonian dynamics (too massive body in a very distant circular orbit around the Sun). Hence the effect of MD should be distinguishable from that of the distant planet in simulations done on large timescales.

3. Models

In § 3.1 the adopted model of the Milky Way matter distribution is presented and in § 3.1.1 the appropriate PMD for this model is calculated. Such ‘complicated’ model is considered solely in order to estimate matter density in the solar neighborhood and hence estimate the effect of the Galactic tide, see §§ 3.1.3, 5 and 6. In § 3.2 the simplified model of the MOC embedded in constant external field is introduced. Majority of the qualitative analysis performed in the paper is carried under the assumption

of this simple model. Moreover, it will be shown that the Galactic tide is of much less importance for MOC comets than for the classical OC comets.

Firstly, we erect a rectangular Galilean coordinate system $O_\odot(\xi', \eta', \zeta')$ centred on the Sun. At time $t = 0$ (present time) the inertial reference frame $O_\odot(\xi', \eta', \zeta')$ coincides with the rotating Galactic rectangular coordinate system, i.e. ξ' axis is directed from the Sun to the GC at $t = 0$. We also use an inertial frame centred on the GC, denoted $O_{GC}(x, y, z)$, with $x - y$ plane being the Galactic plane and x axis directed from the GC to the Sun at $t = 0$.

3.1. Milky Way

We adopt the Milky Way mass model of McGaugh (2008), the similar one as in Lüghausen et al. (2014). McGaugh (2008) concluded that MOND prefers short disk scale lengths in the range $2.0 < r_d < 2.5$ kpc. The modelled Milky Way consists of a stellar double-exponential disk with the scale length $R_d = 2.3$ kpc and the scale height $z_d = 0.3$ kpc with the disk mass $4.2 \times 10^{10} M_\odot$. Moreover it has a thin gas disk of the total mass $1.2 \times 10^{10} M_\odot$ with the same scale length and half scale height as the stellar one and a bulge modelled as a Plummer’s sphere with the mass $0.7 \times 10^{10} M_\odot$ and the half-mass radius 1 kpc.

3.1.1. Phantom matter density

MD predicts complex structure of ‘Newtonist’s dark halo’ with a pure disk component and rounder component with radius-dependent flattening that becomes spherical at large distances (Milgrom 2001), see also Fig. 5 in Lüghausen et al. (2015).

We have calculated PMD of the Milky Way model according to the numerical scheme of § 2.2. Cartesian (x, y, z) grid with $512 \times 512 \times 256$ cells and resolution of $0.1 \times 0.1 \times 0.02$ kpc was used. This resolution was tested to be sufficiently fine enough that the calculated PMD changes negligibly if the resolution is further increased. Fig. 2 shows the vertical PMD $\rho_{ph}(z)$ at $R = R_0 = 8.3$ kpc within $|z| < 1$ kpc. The K_z force perpendicular to the Galactic plane will be obviously enhanced in this case, compared to the Galaxy residing in a spherical DM halo, as predicted by Milgrom already in his pioneer paper (Milgrom 1983b).

Due to small stellar samples (Hipparcos data) one cannot precisely recover the shape of $K_z(z)$ or of the dynamical density, only the surface density below some $|\bar{z}|$, where \bar{z} is the mean distance of the samples from the Galactic plane (Bienaymé et al. 2009). We should compare the calculated surface density of the baryonic matter plus the phantom matter with observations. Holmberg & Flynn (2004) found the dynamical surface density $\Sigma_0 = 74 \pm 6 M_\odot \text{pc}^{-2}$ within $|z| < 1.1$ kpc. By fitting the calculated local PMD with superposition of three exponential disks we have found $\Sigma_0 = 80 M_\odot \text{pc}^{-2}$ within $|z| < 1.1$ kpc, consistent with the value of Holmberg & Flynn (2004). The portion $43 M_\odot \text{pc}^{-2}$ resides in the normal matter and $37 M_\odot \text{pc}^{-2}$ in the phantom.

3.1.2. Dark matter halo of Newtonian Galaxy

The Navarro-Frenk-White (NFW) halo model (Navarro et al. 1997):

$$\rho_h = \frac{\rho_{h,0}}{\delta(1 + \delta)^2}, \quad (15)$$

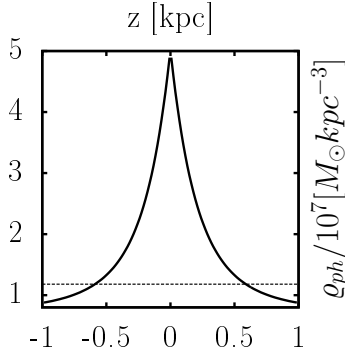


Fig. 2. PMD of the Milky Way (solid) modelled as in § 3.1 at $R = R_0 = 8.3$ kpc within $|z| < 1$ kpc. NFW dark matter density (dashed line) is also depicted.

where $\delta \equiv r/r_h$, r_h is the scale radius (spherically symmetric halo, r is radial coordinate), $\varrho_{h,0}$ is a constant, represents culmination of the present day theoretical knowledge in the standard CDM based cosmology.

In § 6 we want to compare the effect of the Galaxy on the MOC and the classical OC. We use the NFW model as the model of the Milky Way dark matter halo in the Newtonian framework in order to find local mass density in the solar neighborhood and quantify the Galactic tide.

CDM haloes are routinely described in terms of their virial mass M_{vir} , which is the mass contained within the virial radius r_{vir} , and the concentration parameter $c = r_{-2}/r_{vir}$, where r_{-2} is the radius at which the logarithmic slope of the density profile $d \log \varrho_h / d \log r = -2$ (for the NFW profile, $r_{-2} = r_h$). The virial radius r_{vir} is defined as the radius of a sphere centred on the halo centre which has an average density Δ times the critical density $\varrho_{crit} = 3H_0^2/(8\pi G)$, where H_0 is the Hubble constant. Δ varies with redshift, with $\Delta \approx 100$ today. For the NFW model

$$\frac{\varrho_{h,0}}{\varrho_{crit}} = \frac{\Delta}{3} \frac{c^3}{\ln(1+c) - c/(1+c)} \quad (16)$$

holds. Thus knowing the concentration parameter c we can find $\varrho_{h,0}$ of Eq. (15). Boylan-Kolchin et al. (2010) examined (NFW) haloes taken from the Millennium-II simulations at redshift zero, in the mass range $10^{11.5} \leq M_{vir} [h^{-1} M_\odot] \leq 10^{12.5}$, a mass range that the Milky Way's halo is likely to lie in, and determined that the probability distribution of the concentration parameter was well fitted by a Gaussian distribution in $\ln c$, with $\langle \ln c \rangle = 2.56$ and $\sigma_{\ln c} = 0.272$. We adopt $c = \exp(2.56)$ to be the concentration parameter of the Galaxy. The remaining degree of freedom in Eq. (15), represented by the scale radius r_h , can be eliminated by fitting the circular speed V_0 at radial distance R_0 : $V_0^2 = V_{d,s}^2 + V_{d,g}^2 + V_b^2 + V_h^2$, where the added squared speeds represent particular Galactic components (stellar disk, gas disk, bulge, dark halo) determined by the particular masses enclosed within R_0 . Doing so for $V_0 = 240$ km/s, $R_0 = 8.3$ kpc we find: $\varrho_{h,0} = 5.750 \times 10^6 M_\odot \text{ kpc}^{-3}$, $r_h = 28.4$ kpc. Surface density of the NFW halo within $|z| < 1.1$ kpc is $26 M_\odot \text{ pc}^{-2}$, consistent with the lower bound on Σ_0 (Holmberg & Flynn 2004).

3.1.3. Galactic tide

We use a 1D model of the Sun's motion through the Galaxy with the Sun moving in a circular orbit upon which are superimposed small vertical oscillations. For the vertical (perpendicular to the

Galactic midplane) acceleration of the Sun at $z = z_\odot$ we assume

$$\ddot{z}(z_\odot) = -\frac{\partial \Phi}{\partial z}(z_\odot) = -4\pi G \int_0^{z_\odot} \varrho(z) dz, \quad (17)$$

where in MD, $\varrho(z) = \varrho_b(z) + \varrho_{ph}(z)$, is the local vertical 'matter density' which is sum of the baryonic and the phantom density at $R = R_0$ and Φ is the QUMOND potential of the Galaxy, see § 2.2 and § 3.1. In Newtonian dynamics, $\varrho(z) = \varrho_b(z) + \varrho_h(z)$, where $\varrho_h(z)$ is vertical density of the DM halo at $R = R_0$. Eq (17) hangs on the fact that the rotation curve of the Galaxy is approximately flat at the position of the Sun - for an axisymmetric model of the Galaxy: $(1/R)\partial(R\partial\Phi/\partial R)/\partial R + \partial^2\Phi/\partial z^2 = 4\pi G\varrho(R, z)$ with $\partial(R\partial\Phi/\partial R)/\partial R \approx 0$ holds. Fig. 3 shows oscillation of the Sun through the Galactic disk governed by Eq. (17). The oscillations has period 76.7 Myr. The model of the Galaxy of § 3.1 is employed.

We approximate the tidal acceleration of a comet¹² in the inertial frame of reference $O_\odot(\xi', \eta', \zeta')$ centred on the Sun as $(0, 0, \ddot{\zeta}'_{tide} \equiv \ddot{z}_c - \ddot{z}_\odot)$ with

$$\ddot{\zeta}'_{tide} = -4\pi G\varrho(z_\odot)\zeta' + O(\zeta'^2), \quad (18)$$

where z_c and z_\odot are vertical components (perpendicular to the Galactic midplane) of the position vector of the comet and the Sun with respect to the GC and $z_c = z_\odot + \zeta'$ holds. We omit the ξ' and η' components of the tide as these are approximately an order of magnitude smaller than the ζ' component (Heisler & Tremaine 1986). Note that this is true not only in Newtonian dynamics but also in MD as the distribution of the phantom matter resembles that of a disk close to the galactic midplane.

3.2. Simple model of the Milgromian Oort cloud

Here we introduce a simple model of the MOC embedded in external field of constant magnitude (no tides). Accounting for the external field is necessary step as in MD the external field does not decouple from the internal dynamics.

We assume that the Sun travels with angular frequency $\omega_0 = V_0/R_0$ in a circular orbit of radius R_0 which lies in the Galactic midplane ($z = 0$).

Let the Newtonian external field of the Galaxy at the position of the Sun be approximated by the time-dependent vector:

$$\mathbf{g}_e^N = [g_e^N \cos(\omega_0 t), g_e^N \sin(\omega_0 t), 0] \quad (19)$$

in $O_\odot(\xi', \eta', \zeta')$. So that at $t = 0$: $\mathbf{g}_e^N = g_e^N \hat{\xi}'$, where $\hat{\xi}'$ is the unit vector. In Eq. (19) we assume that the Sun orbits counterclockwise in the plane $\xi' - \eta'$ of $O_\odot(\xi', \eta', \zeta')$.

In Eq. (6) we now have $\nabla\phi_{S.S.}^N = GM_\odot\Xi'/\Xi'^3 - \mathbf{g}_e^N$, where $\Xi' = [\xi', \eta', \zeta']$, $\Xi' \equiv (\xi'^2 + \eta'^2 + \zeta'^2)^{1/2}$ and the lower index 'S.S.' stresses that we are dealing with the Solar System embedded in the external field of the Galaxy. For the PMD we thus obtain:

$$\varrho_{ph,S.S.} = \frac{\nabla\tilde{v} \cdot (GM_\odot\Xi'/\Xi'^3 - \mathbf{g}_e^N)}{4\pi G}, \quad (20)$$

where $\tilde{v} \equiv \tilde{v}(|GM_\odot\Xi'/\Xi'^3 - \mathbf{g}_e^N|/a_0)$, using that $\nabla\phi_{S.S.}^N$ is divergenceless vector field. Phantom potential $\phi_{ph,S.S.}$ can be found by solving ordinary Poisson equation

$$\Delta\phi_{ph,S.S.} = 4\pi G\varrho_{ph,S.S.}, \quad (21)$$

¹² MD is non-linear. One cannot a priori sum up partial accelerations to get a net acceleration vector. The usage of Eq. (18) in MD is further discussed and justified in § 5.

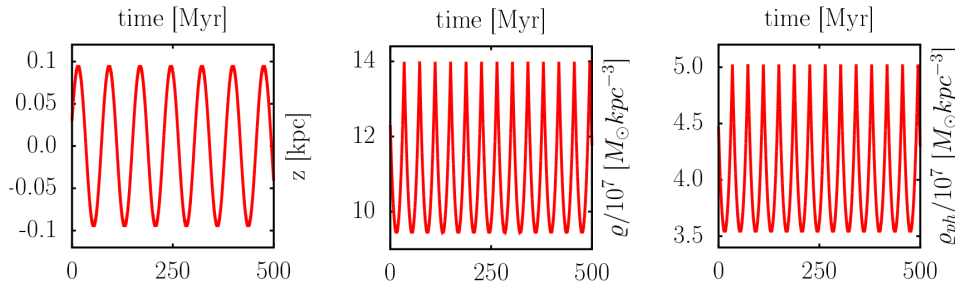


Fig. 3. **Left:** Oscillation of the Sun governed by Eq. (17) in MD. We have used $z_{\odot}(0) = 30$ pc and $v_{z_{\odot}}(0) = 7.25$ km s⁻¹ as the initial conditions of the Sun’s motion. **Middle:** Local ‘total matter density’ $\rho = \rho_b + \rho_{ph}$ as experienced by the oscillating Sun. **Right:** Local PMD as experienced by the oscillating Sun.

with the boundary condition: $\phi_{ph,S.S.} = -\mathbf{g}_e \cdot \Xi'$. The equation of motion in $O_{\odot}(\xi', \eta', \zeta')$ then reads

$$\ddot{\Xi}' = -\nabla\Phi_{S.S.} - \mathbf{g}_e, \quad (22)$$

where $\Phi_{S.S.} = -GM_{\odot}/\Xi' + \phi_{ph,S.S.}$.

As QUMOND equations are linear when formulated with aid of phantom matter we can also look for a solution of Eq. (21) with the vacuum boundary condition ($\phi_{ph,S.S.} = 0$ at the boundary) and then evolve a body with

$$\ddot{\Xi}' = -\nabla\Phi_{S.S.}. \quad (23)$$

3.2.1. Simple model of the Oort cloud - numerical solution at $t=0$

For integration of cometary orbits throughout the paper we employ the well-tested RA15 routine (Everhart 1985) as part of MERCURY 6 gravitational dynamics software package (Chambers 1999), which we have appropriately modified to be compatible with MD framework. Eq. (19) has to be transformed from $O_{\odot}(\xi', \eta', \zeta')$ to coordinate system used by MERCURY 6. Such transformation and subsequent modification of Eqs. (20) and (22) are straightforward. $O_{\odot}(\xi, \eta, \zeta)$ denotes from now on the rectangular coordinate system we use in MERCURY 6, i.e. Galilean coordinates coinciding at $t = 0$ with the heliocentric ecliptical coordinate system¹³.

During short time periods, compared to the period of the Sun’s revolution around the GC, ~ 210 Myr, one can approximate Eq. (19) with the constant vector $\mathbf{g}_e^N = [g_e^N, 0, 0]$, $g_e^N \approx 1.22 a_0$, in $O_{\odot}(\xi', \eta', \zeta')$. We have used this approximation in order to find phantom potential $\phi_{ph,S.S.}$ experienced by a body in the MOC model represented by Eqs. (19) - (22). The numerical procedure is analogous to the one described in § 2.2. The boundary conditions are described under Eq. (21). We have employed a regular Cartesian grid with 512³ cells and resolution of 390 au centred on the Sun. This resolution was tested to be sufficiently fine enough that the trajectories of comets does not change significantly if the resolution is further increased. In the case of inner OC orbits in §§ 6.2 and 7.1 we have used resolution of 78 au with the same result. The calculated phantom acceleration, $-\nabla\phi_{ph,S.S.}$, is linearly interpolated to instantaneous position of the body within each integration cycle. We refer to this simplified dynamical model of the MOC as ‘simple model of the MOC’.

¹³ $O_{\odot}(\xi', \eta', \zeta')$ vs. $O_{\odot}(\xi, \eta, \zeta)$, primed are Galactic and not-primed are ecliptic coordinates at $t = 0$.

3.3. Escape speed

In MD is an isolated point mass M at distance $r \gg (GM/a_0)^{1/2}$ source of the potential of the form

$$\Phi(r) \sim (GMa_0)^{1/2} \ln(r). \quad (24)$$

Eq. (24) yields asymptotically flat rotation curves but also the fact that there is no escape from the central field produced by the isolated point mass in MD, since $V_{esc}^2(r) \sim \Phi(\infty) - \Phi(r)$. But, external field (which is always intrinsically present) actually regularizes former divergent potential, so that it is possible to escape from non-isolated point masses in MD (Famaey et al. 2007), as we have already seen in § 2.3.

Escape speed of a comet can be well defined as (Wu et al. 2007, 2008)

$$V_{esc}(\xi, \eta, \zeta) = \sqrt{-2\Phi_i(\xi, \eta, \zeta)}, \quad (25)$$

with $-\nabla\Phi_i = \ddot{\Xi}$. The estimate of the escape in the direction perpendicular to the external field can be found by approximating Galactic EFE acting on OC with the simple curl-free formula of Eq. (13), where now $\mathbf{g}_i = -GM_{\odot}\Xi/\Xi^3$. For escape speed at $\Xi = r_c$ we then have

$$V_{esc}(r_c) = \left[2 \int_{r_c}^{\infty} g_i(\Xi) d\Xi \right]^{1/2}, \quad (26)$$

where $g_i(\Xi) \equiv |\ddot{\Xi}|$. We use Eq. (26) in § 4.1 and § 4.2 in order to estimate binding energy of a comet.

4. Oort cloud as seen by Milgromian astronomer

Do the observations lead us to hypothesize the existence of a vast cloud of bodies as a reservoir of new comets also if we interpret the data with the laws of MD? If it is so, how vast and shaped, in rough sense, should be the cloud compared to the classical one?

DK11 studied dynamical evolution of 64 Oort spike comets with orbits determined with the highest precision, discovered after 1970, having their original semi-major axes larger than 10 kau and osculating perihelion distances $q > 3$ au (to minimize non-gravitational effects). They identified 31 comets as dynamically new (having their first approach to the zone of significant planetary perturbations; for the detailed definition see the paper), and one of these comets as possibly hyperbolic¹⁴. Median value of the original reciprocal semi-major axis for the 30 comets

¹⁴ DK11 found the original reciprocal semi-major axis of the comet C/1978 G2 to be $-22.4 \pm 37.8 \times 10^{-6}$ au⁻¹.

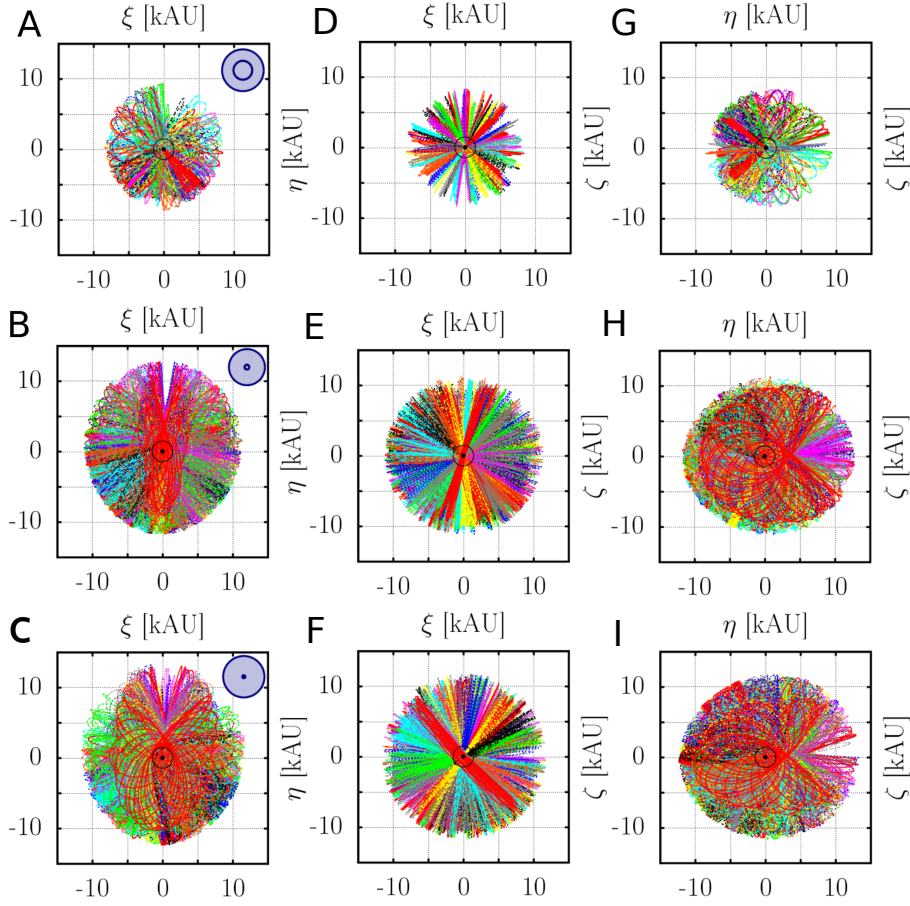


Fig. 4. Past Milgromian trajectories of 3×100 Monte Carlo particles projected to 3 mutually orthogonal planes of $O_{\odot}(\xi, \eta, \zeta)$. The particles were initialised with original Newtonian orbital elements: $a = 10$ (top row), 50 (middle row), 100 (bottom row) kau, q distributed uniformly on the interval $(0, 8)$ au, $\cos(i)$ distributed uniformly on the interval $(-1, 1)$, ω and Ω distributed uniformly on the interval $(0, 2\pi)$, among the particles, and mean anomaly $M = 0$. Then the particles were evolved back in time in the simple model of the MOC, § 3.2, for one Keplerian period (≈ 1 Myr) in the case of $a = 10$ kau and for 10 Myr in the case of $a = 50$ and 100 kau. The concentric circles at the top right corner of figures A,B and C represent relative radii of the Milgromian (always the smaller circle) and Newtonian OC (radius = $2a$; always the larger circle) as determined by the simulation and assuming that the cloud is the smallest sphere encompassing all orbits of given initial a . At $[0,0]$ resides the Sun as indicated by the symbol.

on the certainly bound orbits is $22.385 \times 10^{-6} \text{ au}^{-1}$ what corresponds to 44.7 kau, maximum and minimum values in the sample read 250.6 and 21.9 kau respectively. All the orbits have osculating $q < 9$ au. The orbits of dynamically new comets are free from planetary perturbations and can be used to study the source region of these comets. We emphasize that for a comet being dynamically new under Newtonian dynamics does not necessary mean to be dynamically new under MD. Reconsideration of the dynamical status in MD would require similar approach as in DK11 with extensive usage of orbital clones to cover the large errors in original orbital energy determination.

To acquire vital motivation we have used more straightforward approach as a first step. Employing the aforementioned simple model of the MOC we have traced past trajectories of 300 Monte Carlo test particles representing a sample of Oort spike comets. We consider fairly small sample as in reality observed samples are of similar or even smaller numbers. We have considered three values of particle's initial semi-major axis $a = 10, 50$ and 100 kau. For each of the three values of a we have initialised 100 test particles at their perihelia - all the perihelia lie in the deep Newtonian regime - with the following randomly generated original Newtonian orbital elements: q distributed uni-

formly on the interval $(0, 8)$ au, $\cos(i)$ distributed uniformly on the interval $(-1, 1)$, ω and Ω distributed uniformly on the interval $(0, 2\pi)$, among the test particles, here q is perihelion distance, i is inclination with respect to the ecliptics, ω is argument of periaapsis and Ω is longitude of the ascending node. The initial Newtonian orbital elements are immediately transformed into the initial Cartesian positions and velocities, the notions independent on the dynamical framework; also these are the observables on the basis of which are the orbital elements calculated¹⁵. We have followed the particles with $a = 10$ kau back in time for one Keplerian period (which is by no means the real period assuming MD), $2\pi (a[\text{au}])^{3/2}/k$ days, where k is Gaussian gravitational constant, and the particles with $a = 50$ and 100 kau for 10 Myr. We do not use integration time of one Keplerian period in the latter case because during this time the external field would change its direction non-negligibly ($a = 100$ kau orbit has the Keplerian period $T_{Kep} \approx 32$ Myr). Anyway, as will be shown all the particles with initial $a = 50$ and 100 kau revolve many times during 10 Myr.

¹⁵ Published catalogues and papers usually offer only the Newtonian orbital elements, not the observables.

By the term ‘original orbit’ we want to emphasize the fact that in reality the outer planets and non-gravitational effects are important dynamical agents, changing primarily value of the semi-major axis. We can imagine the ensemble of the initial orbital elements as the result of backward integration of observed osculating (instantaneous) orbits to the time when the comets/particles enter the planetary zone.

The past QUMOND trajectories of the particles are shown in Fig. 4. Trajectories can be typically described as ellipses with quickly precessed line of apsides. Moreover, the external field often changes perihelion distances of the particles rapidly and almost irrespective of their initial semi-major axis. This important fact is discussed in § 6. In this case the orbits change its shape dramatically as was previously illustrated in Iorio (2010a) for the deep-MD orbits only.

Small departure from the isotropy of the cloud can be seen in Fig. 4. The cloud is prolonged in the direction of the η axis. Also indistinct pac-man shape of ξ - η and η - ζ plane cuts is emerging. This is because of the external field of the Galaxy which points in the direction of $-\hat{\mathbf{x}}$ of $O_{GC}(x, y, z)$ (the direction Sun-GC at $t = 0$), what corresponds to the direction of $-\hat{\boldsymbol{\eta}}$ of $O_{\odot}(\xi, \eta, \zeta)$. The gravity is stronger at negative η than at positive. This can be the most easily noticed on $\nu(\beta)$ dependence on the vector sum in grossly approximative formula $\mathbf{g}_i = \nu(|\mathbf{g}_i^N + \mathbf{g}_e^N|/a_0)\mathbf{g}_i^N$ (note that larger β means smaller $\nu(\beta)$). Also note the smaller precession rate of the projected orbits in $\xi - \zeta$ plane. This is again because the ξ and ζ components of the Galactic external field are much smaller than the η component.

Anyway, the most important results is that even the orbits with initial $a = 100$ kau are confined in a cube of side ~ 28 kau. The Newtonian cube would be in this case of side ~ 400 kau. This implies that the OC as revealed by comets with original $0 < a < 100$ kau and interpreted by MD could be much more compact than the Newtonian one.

These findings looks problematic for MD at first sight. The classical picture of the Galactic tide, as the most effective comet injector, is that the sufficient decrease in comet’s perihelion distance during one revolution - to be able to penetrate the Jupiter-Saturn barrier - can be made only for comets with $a > 20 - 30$ kau (e.g., Levison et al. 2001; Rickman 2014), hence the comets with aphelion distances larger than 40 - 60 kau if eccentricity is close to 1. These are much larger heliocentric distances than those comets encounter in MOC. Also comets of the classical inner OC taking advantage of the Jupiter-Saturn barrier, by inflating their semi-major axes, come through this outer region ($a > 20 - 30$ kau; i.e. the comets appear to be from the outer OC) where final decrease in perihelion distance is effectively made (Kaib & Quinn 2009). All these findings are of course Newtonian. The tidal field of the Newtonian Galaxy embedded in the DM halo is little different from the QUMOND one, especially its vertical (perpendicular to the Galactic midplane) part. Moreover completely beyond the tides, MD’s EFE can have decisive influence on the dynamics. We address this issue more rigorously in § 6, where injection of the bodies from the inner OC (in the classical jargon) is studied. As MD enhances binding energy of a comet the classical effect of the Jupiter-Saturn barrier has to be actually revised, see § 4.2. Last but not least we have to stress that the steady-state distribution of the bodies in the cloud could look different in MD, see discussion in § 8.

4.1. Escaping comets?

We use the term ‘hyperbolic comet’ for a comet whose Newtonian two-body orbital energy is positive and which is according

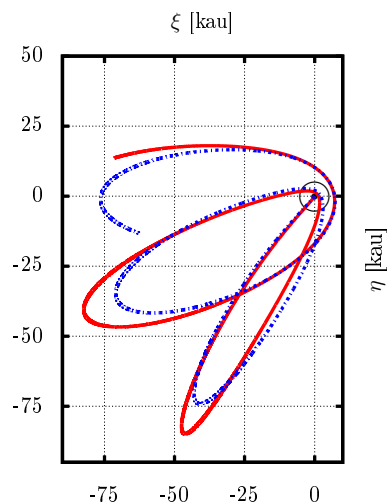


Fig. 5. Past trajectories of two slightly hyperbolic comets in the simple model of the MOC. Both were initialised at their perihelia, one with $q = 8$ au, $e = 1.00150$, $\omega = \pi/4$ (solid line), the other with $q = 3$ au, $e = 1.00055$, $\omega = \pi/4$ (dot-dashed line). All the other orbital elements were set to 0. Integration time was 20 Myr. As can be seen these comets are bound (returning) in MD. At [0,0] resides the Sun as indicated by the symbol.

to a Newtonian astronomer not bound (not returning) to the Solar System. In this section we investigate the idea that slightly hyperbolic comets can be bound to the Milgromian Solar System, as first pointed out by Milgrom (1986b).

The statistics of the original reciprocal semi-major axes, $1/a_{orig}$, reveals, besides the famous Oort spike, also a small but non-negligible number of slightly hyperbolic comets (e slightly larger than 1; e.g., Fig. 1b in Dones et al. (2004)). These are usually considered to follow very eccentric elliptic orbits in reality, rather than to be interstellar intruders, but due to observational errors or inappropriate modelling of non-gravitational forces they seem to move on the hyperbolic orbits (Dones et al. 2004). Thanks to the boosted gravity in MD the slightly hyperbolic comet could be still bound to the Solar System¹⁶.

Comparing the escape speed at perihelion, $V_{esc}(q)$, see Eqs. (13) and (26), with the tangential speed at the perihelion, $V_{peri}(e, q)$, we can decide whether a comet is bound or not. $V_{peri}(e, q)$ can be computed in the usual way. We are at the perihelion - in the deep Newtonian regime, and it depends only on the local gravitational field. Opposite case is the escape speed which has to be calculated from the MD gravity no matter where we start from, see Eq. (26). Assuming motion in the ecliptic plane, $i = 0$, we have:

$$V_{peri} = \sqrt{\frac{GM_{\odot}}{q}} (1 + e). \quad (27)$$

Radial speed at the perihelion is 0. Thus for a given q we can find the limiting eccentricity e_{lim} , so $e > e_{lim}$ implies $V_{peri}(e, q) > V_{esc}(q)$. For example $q = 3$ au implies $e_{lim} = 1.00075$ and $q = 8$ au leads to $e_{lim} = 1.00199$. Slightly hyperbolic comets with $e < e_{lim}$ are bound in MD. Fig. 5 shows trajectories of two comets initialised with the orbital elements $q = 3$ au,

¹⁶ To be thorough, in Newtonian dynamics, it is vice-versa possible for a comet to appear to be bound but to originate in the interstellar space as a result of the Galactic tidal influence (Neslušan & Jakubík 2013). Anyway, this special configuration is highly improbable (Neslušan & Jakubík 2013).

$e = 1.00055$, $\omega = \pi/4$ (all the other elements are set to 0) and $q = 8$ au, $e = 1.00150$, $\omega = \pi/4$ (all the other elements are set to 0) and then integrated backwards for 20 Myr assuming the simple model of the MOC. This is quite long time interval to assume stationarity of the external field, thus the real trajectories would be a little different as the external field changes its direction. Anyway we just intent to illustrate as slightly hyperbolic comets are bound in MD and this qualitative result remains the same.

Observations of comets with similar original orbital elements could inflate the former conservative estimate of the MOC size to sizes comparable with the classical OC. In § 5 we take real cometary data and look what they say about the size and shape of the MOC.

4.2. Does Jupiter and Saturn act as a barrier in MD?

The enhanced binding energy of MOC comets raises a question: how the mechanism of the planetary barrier operating in the classical OC change in the MD case?

QUMOND conserves energy. We use Eqs. (13) and (26) to approximate QUMOND and assume energy conservation. Let us have a comet at perihelion, lying deeply in the Newtonian regime, with kinematics characterized by the Newtonian orbital elements a and q . We can find its specific binding energy in MD, simply as

$$E_{BM} = -\frac{1}{2} \left[V_{pert}^2(a, q) - V_{esc}^2(q) \right], \quad (28)$$

where we can use Eq. (27) under the assumption $i = 0$. Note that we have put minus sign in front of the factor 1/2 on the RHS of Eq. (28) because the binding energy is defined as a positive number. For comets with $a = 10, 50$ and 100 kau the ratio E_{BM}/E_{BN} , where $E_{BN} = [GM_{\odot}/(2a)]$ is the Newtonian binding energy per unit mass, is approximately equal to 3, 13 and 26 respectively. Using the 1D QUMOND approximation, Eq. (60) in Famaey & McGaugh (2012), instead of Eq. (13), these ratios are 2, 7 and 13 respectively. For near-parabolic orbits the value of E_{BM} depends only weakly on q .

Comet of the classical OC in, let say typical, $a = 50$ kau orbit experiences energy change per perihelion passage proportional to its own binding energy¹⁷ at $q \sim 15$ au, see Fig. 1 in Fernández & Brunini (2000). Making the binding energy of this comet in MD ~ 10 times larger this criterion is met at $q \sim 7$ au. Roughly speaking this means that MOC comets with $q < 7$ au, instead of the classical value ~ 15 au, are removed from the cloud due to planetary perturbations. The planetary barrier similarly to the whole cloud shifts inward in MD. Anyway it can still act in a way of inflating semi-major axes for those comets having $q > 7$ au, but these are not a priori prevented from being injected inside the inner Solar System as in the case of the removed comets of the classical OC.

5. Observed near-parabolic comets in Milgromian dynamics

Motivated by the crude picture of the OC outlined in § 4, we have used real cometary data to investigate origin of the near-parabolic comets in the framework of MD.

¹⁷ This certainly depend on the orbital inclination, as can be seen in Fig. 1 in Fernández & Brunini (2000). The footnoted sentence is true for highly inclined orbits with $i \in (120, 150)$ deg. For orbits close to ecliptics the planetary kick at 15 au is about 6 times larger.

We have approximated action of QUMOND by the simple model of the MOC, with the constant external field of the Galaxy \mathbf{g}_e coupled to the QUMOND equations, see § 3.2. The rotation of \mathbf{g}_e has period of ~ 210 Myr, therefore we use integration times to be Keplerian periods for those comets having these lesser than 10 Myr. For those that have Keplerian periods larger than 10 Myr we use integration time of 10 Myr as all these have much shorter real (QUMOND) ‘periods’, i.e. times between two successive perihelia. Moreover, the tidal effect, which comes from the Galactic gravity gradient across the OC, is also accounted. The Galactic tide model is described in § 3.1.3. This model reflects the local density of the baryonic + phantom matter as determined by QUMOND for the adopted baryonic model of the Galaxy, see §§ 2.2 and 3.1. We have simply added the tidal acceleration $(0, 0, \ddot{\zeta}_{tide})$, Eq. (18), to RHS of Eq. (22). This is only approximation in nonlinear MD. But, it proves to be good idea to model EFE (assuming spatially invariant field) and tides as two separate effects of the Galaxy, see §§ 5.2 and 6.1.

We have taken the original orbits from the sample of near-parabolic comets that were identified as dynamically new in DK11, convert them to initial positions and velocities of test particles and integrate these back in time, looking for their past Milgromian trajectories.

5.1. Data

Our sample consists of those 31 comets identified as dynamically new in DK11. We have omitted errors in lengths of original semi-major axes a_{orig} , the only orbital element with significant error, and rather took only their expected values as these are fairly typical for the Oort spike comets. More exact approach should proceed in a similar manner as DK11 did, covering error in the orbital energy determination with large number of virtual orbits, but this is much more processor-time consuming in MD than in Newtonian dynamics.

The sample contains also one slightly hyperbolic comet, C/1978 G2, with perihelion $q = 6.28$ au and eccentricity $e = 1.00014083$. Also note orbit of the comet C/2005 B1 with very large semi-major axis of 250.6 kau.

Original orbital elements of the sample comets were retrieved from Królikowska (2014) and are displayed in Table 1. These were calculated at heliocentric distance 250 au, still well in the Newtonian regime.

5.2. Results

The past QUMOND trajectories of the sample comets are shown in Fig. 6. The resulting size and overall shape of the MOC is in large agreement with the one obtained in § 4. The trajectory of the single comet with $e > 1$ in our sample, C/1978 G2, is redrawn in Fig. 7. In Milgromian framework the comet is bound, visiting similar heliocentric distances as the other comets in our sample.

In MD we expect the Galactic tide to be stronger than in the Newtonian dynamics, see Fig. 2 and § 3.1.3. However, the changes in orbits - perihelia positions and precession rates - induced by the Galactic tide are negligible compared to those induced by the EFE, see also § 6. Figs. 6 and 7 would not look different if the Galactic tide model as presented in § 3.1.3 would not be incorporated. This is a natural consequence of the compactness of the cloud. The comets cruise up to $\Xi \sim 13$ kau where the tidal torquing is still minute but EFE plays a dominant role. As mentioned above we do model the EFE and the Galactic tide as the separate effects.

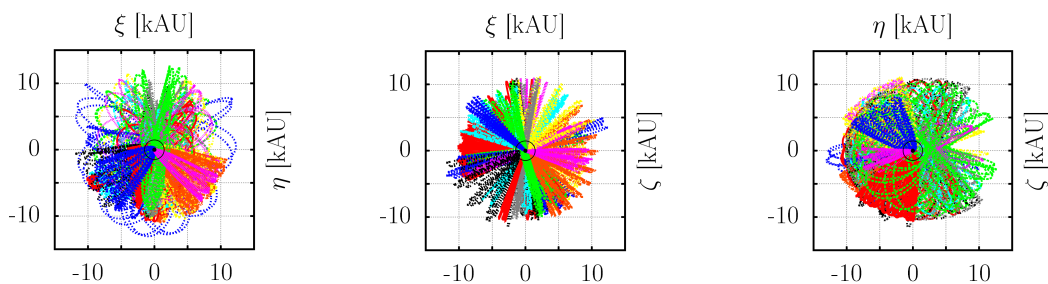


Fig. 6. Past Milgromian trajectories of 31 near-parabolic comets, those identified as dynamically new in DK11, projected to 3 mutually orthogonal planes of $O_{\odot}(\xi, \eta, \zeta)$. Dynamical model of the OC consists of the stationary Galactic field coupled to the QUMOND equations, see § 3.2, and the Galactic tide model, see § 3.1.3. The comets with Keplerian periods T_{Kep} lesser than 10 Myr were followed for the time of T_{Kep} , those with $T_{Kep} > 10$ Myr were followed for 10 Myr. Inferred MOC is much smaller than the classical OC, see Table 1 for comparison with Newtonian orbits. At [0,0] resides the Sun as indicated by the symbol.

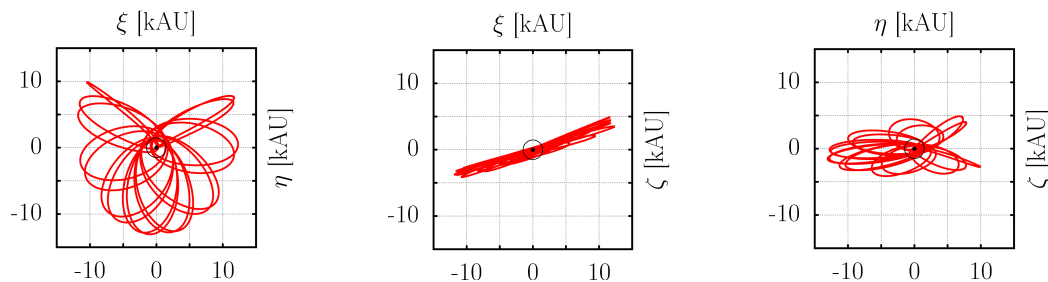


Fig. 7. Past Milgromian trajectory of the comet C/1978 G2, the slightly hyperbolic comet. Initial $q = 6.28$ au and $e = 1.00014083$. At [0,0] resides the Sun as indicated by the symbol.

In Fig. 8 we show specific angular momentum as a function of time, $L(t)$, for the comet C/1974 V1 in the simple model of the MOC. Tides are omitted this time. Periodic changes in angular momentum are induced purely by EFE. Similar behaviour can be found also by checking the other comets in the sample. Taking into account the Galactic tide has only minor effect and $L(t)$ is very much the same.

6. Galactic torque

We have shown that MOC is much smaller than the classical OC. MOC boundary, as found by tracing Oort spike comets with initial eccentricity $e < 1$ (what is the vast majority of the observed comets) back in time, lies at heliocentric distances corresponding to the classical inner OC. Also the single comet with $e > 0$ in § 5 sample, C/1978 G2, orbits in bound orbit at similarly small heliocentric distances in MD. It is presumed that the tidal force at these heliocentric distances is not large enough to decrease perihelion distance sufficiently fast in order for a comet to bypass the Jupiter-Saturn barrier, e.g., Dones et al. (2004). In MD the compactness of the OC does not need to be an obstacle for injection of a comet into the inner Solar System because of the action of EFE.

6.1. Angular momentum change

In this section we preserve the classical idea of the Jupiter-Saturn barrier at ~ 15 au, although in § 4.2 we have shown that the barrier actually shifts inward in MD. Such shift naturally increases the inflow of comets.

To illustrate capability of the EFE to deliver OC bodies into the inner Solar System we have run similar simulation as in § 4. In this case we have intended to mimic sample of comets that

are about to enter/leave the planetary zone. So we have chosen the initial perihelion distance of each particle, q , to be a random number uniformly distributed on the interval (15, 100) au. All the other initial orbital elements of the test particles have been randomly generated in the same way as in § 4. The orbital elements were at $t = 0$ transformed to initial Cartesian positions and velocities, the real observables.

We have employed two distinct dynamical models of the OC, one Milgromian and one Newtonian: (i) the simple model of the MOC, and, (ii) Sun + Galactic tide in the Newtonian framework. We have tested that incorporation of the Galactic tide model as described in Sec. 3.1.3 into the simple model of the MOC has negligible effect for the times corresponding to one revolution of a comet. This is obviously because the comets of the MOC orbit in $\Xi \lesssim 15$ kau, at these heliocentric distances the tidal force is too weak. Two distinct $\varrho(z_{\odot})$ were used: $\varrho(z_{\odot}) = \varrho_b(z_{\odot}) + \varrho_{ph}(z_{\odot})$ in MD and $\varrho(z_{\odot}) = \varrho_b(z_{\odot}) + \varrho_h(z_{\odot})$ in Newtonian dynamics, where $\varrho_b(z_{\odot})$ is local vertical density of baryons and $\varrho_h(z_{\odot})$ is local vertical density of the NFW DM halo.

Figs. 9 ($a = 10$ kau), 11 ($a = 50$ kau) and 13 ($a = 100$ kau) show the heliocentric distance, $\Xi(t)$, and change in magnitude of the specific angular momentum, $\delta L(t) \equiv L(t) - L(0)$, of the particles, as a function of time. The followed time window, T_{rev} , corresponds approximately to one revolution succeeding the perihelion initialisation. In Figs. 10 ($a = 10$ kau), 12 ($a = 50$ kau) and 14 ($a = 100$ kau) we show the value of $\Delta L \equiv L_{max} - L_{min}$ of the individual particles, where $L_{max} \equiv [L(t)]_{max}$ and $L_{min} \equiv [L(t)]_{min}$ are the maximal and the minimal value of $L(t)$ during T_{rev} .

When interpreting these figures we have to bear in mind the timescales of the angular momentum changes, these are ~ 4 ($a = 10$ kau) to ~ 80 ($a = 100$ kau) times smaller in the MOC than in the classical OC. Also note that the particles initialised with a as large as 100 kau are travelling in $\Xi \lesssim 15$ kau in the MOC. It

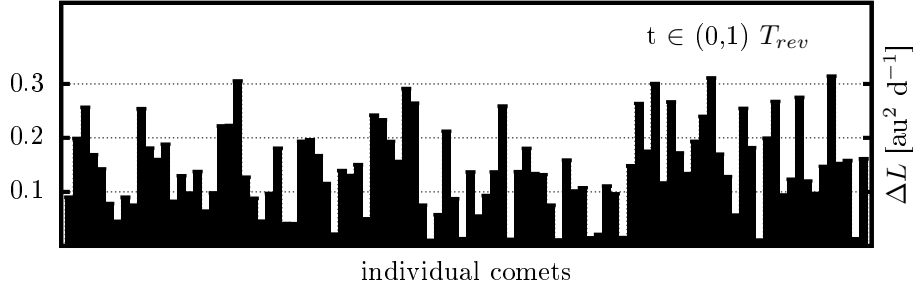


Fig. 10. Histogram of $\Delta L \equiv L_{max} - L_{min}$ for 100 Monte Carlo test particles initialised with $a = 10$ kau and q uniformly distributed on the interval (15, 100) au. Here L_{max} (L_{min}) is maximal (minimal) magnitude of the specific angular momentum as found during one revolution, T_{rev} , succeeding the initialisation of a comet at perihelion. In MD simulation $T_{rev} = 0.26$ Myr, in Newtonian simulation $T_{rev} = T_{Kep}(a = 10 \text{ kau}) \approx 1$ Myr. A single bin corresponds to a single test particle in the simulation. Solid bins are ΔL in the simple model of the MOC, shaded bins (here barely visible), stacked on the solid bins, are ΔL in Newtonian dynamics with gravity of the Sun and the Galactic tide accounted.

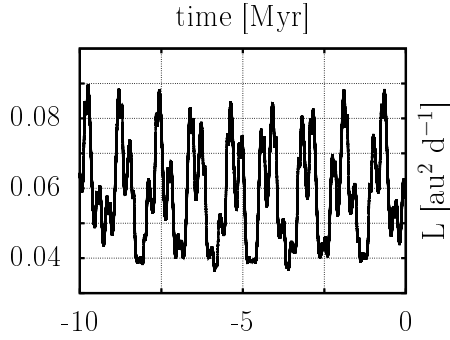


Fig. 8. Specific angular momentum L as a function of time for the comet C/1974 V1. We have assumed the simple model of the MOC (tides are omitted). The periodic changes are induced solely by EFE. The negative time means that we are dealing with the past trajectory of the comet.

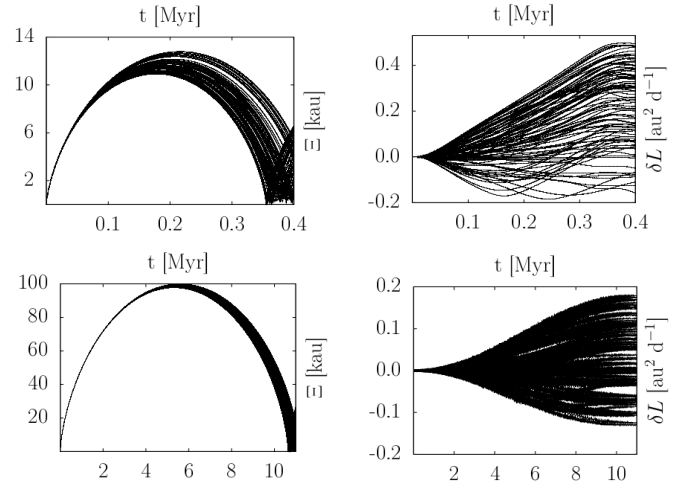


Fig. 11. Same as in Fig. 9 but now the particles were initialised with $a = 50$ kau. The top row represents an output of the Milgromian simulation, the bottom row of the Newtonian simulation. In MD simulation the follow up time, T_{rev} , is set to 0.4 Myr (see top left quarter of this figure for motivation), in Newtonian simulation T_{rev} is set to be the Keplerian period $T_{Kep}(a=50 \text{ kau}) \approx 11$ Myr.

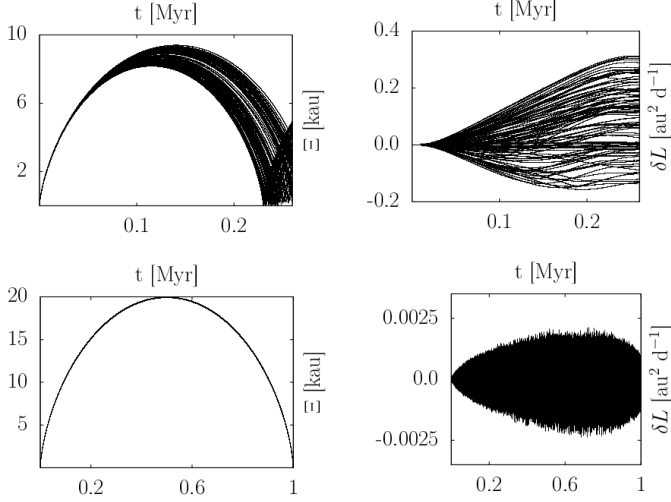


Fig. 9. Heliocentric distance, $\Xi(t)$, and change in magnitude of the specific angular momentum, $\delta L(t) \equiv L(t) - L(0)$, as a function of time, t , for 100 Monte Carlo test particles initialised with $a = 10$ kau and q uniformly distributed on the interval (15, 100) au. The top row represents an output of the Milgromian simulation, the bottom row of the Newtonian simulation. In MD simulation the follow up time, T_{rev} , is set to 0.26 Myr (see top left quarter of the figure for motivation), in Newtonian simulation T_{rev} is set to be the Keplerian period $T_{Kep}(a=10 \text{ kau}) \approx 1$ Myr.

is evident that the injection could be very efficient in the MOC, nevertheless the MOC is much more radially compact than the classical OC. In MD the rapid changes in the angular momentum are induced by EFE. Moreover the bodies that are ‘hidden’ in the classical OC - i.e. not able to reach the observability region, because of either their immunity from the action of the external perturbers, the hypothesized inner core, or, inability to overshoot the Jupiter-Saturn barrier, the inner OC bodies with $a \sim 10$ kau - can be because of EFE delivered from the MOC into the inner Solar System as well, see also § 6.2.

Figs. 12 and 14 show that Newtonian tides (OC) overcome EFE (MOC) in Δq per revolution only for comets with a as large as $\sim 50 - 100$ kau. This is 9 out of 30 comets with $e < 1$ in the § 5 sample.

6.2. Sedna

We have shown that cometary perihelia can be very effectively torqued in and out by EFE even for those comets travelling in fairly small heliocentric distances, ~ 10 kau. Is torquing due

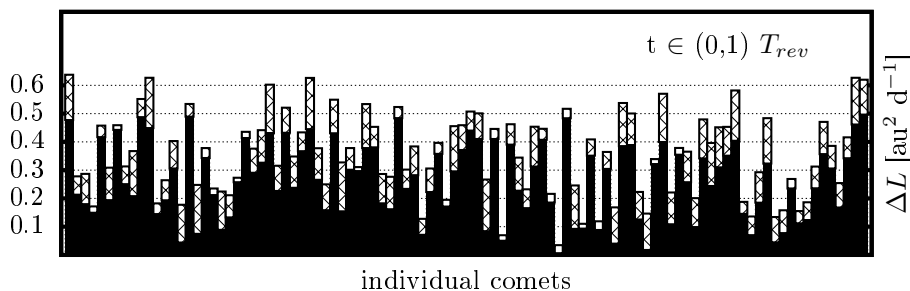


Fig. 12. Same as in Fig. 10 but now the particles were initialized with $a = 50$ kau. In MD simulation $T_{rev} = 0.4$ Myr, in Newtonian simulation $T_{rev} = T_{Kep}(a = 50 \text{ kau}) \approx 11$ Myr. A single bin corresponds to a single test particle in the simulation. Solid bins are ΔL in the simple model of the MOC, shaded bins, stacked on the solid bins, are ΔL in Newtonian dynamics with gravity of the Sun and the Galactic tide accounted.

to EFE important at even smaller heliocentric distances? Can be EFE responsible for the shape of the current puzzling orbit of the trans-Neptunian planetoid Sedna? To address these questions we have run the following simulation: 100 Monte Carlo test particles (Sedna progenitors - Sednitos) with initial $a = 524$ au (Sedna's heliocentric a at epoch 2,457,000.5 JD, according to JPL's service HORIZONS), and among the particles uniformly distributed q in bounds (5, 30) au, i in bounds $(-10, 10)$ deg, ω and Ω in bounds $(0, 2\pi)$, were initialised at their perihelia and then followed for 5.9 Myr in the simple model of the MOC. These initial orbital elements have been chosen in order to mimic the protoplanetary disk origin of Sedna. We have assumed that Sednito's semi-major axis was already pumped to the current Sedna's value at the beginning of the simulation, due to past planetary encounters. The planets were omitted in the simulation.

In Fig. 15 we show $\Delta q \equiv q_{max} - q_{min}$ for 100 simulated Sednitos, where q_{max} and q_{min} are Sednito's maximal and minimal value of q , per 5.9 Myr. As can be seen Δq is in some cases as large as 100 au. At the end of the simulation 7 Sednitos had $q \sim 75$ au, hence very close to the Sedna's perihelion distance. Sedna-like orbits (here simplified as specific a and q values) can be produced by EFE in few Myr. The catch is that as q oscillates in and out on timescales of millions of years the trans-Neptunian bodies with similar orbits as Sedna could possibly wander into the inner Solar System. It is also possible that substantial migrants has been already removed from such orbits and the current population is relatively stable against migration.

Fig. 16 depicts perihelion distance as a function of time for all known bodies with $q > 30$ au and $a > 150$ au in the simple model of the MOC during the next 10 Myr. Initial orbital elements of the bodies were retrieved from Trujillo & Sheppard (2014), see their Table 1 and Extended Data Table 2. Only one of the followed objects, 2010 GB₁₇₄, migrates under 30 au in the next 10 Myr. To investigate migration of these objects thoroughly we would have to improve our dynamical model of the MOC to account for the change in the external field direction, as long integration times would be necessary, and also account for the planetary perturbations. We leave this task to our future study.

7. Varying interpolating function and a_0

Hees et al. (2016) (hereafter H+16) recently constrained most frequently used families of the MD interpolating (transition) function (e.g., § 6.2 in Famaey & McGaugh 2012) with the Cassini spacecraft radio tracking data (Hees et al. 2014). These constraints come from EFE which produces small quadrupole

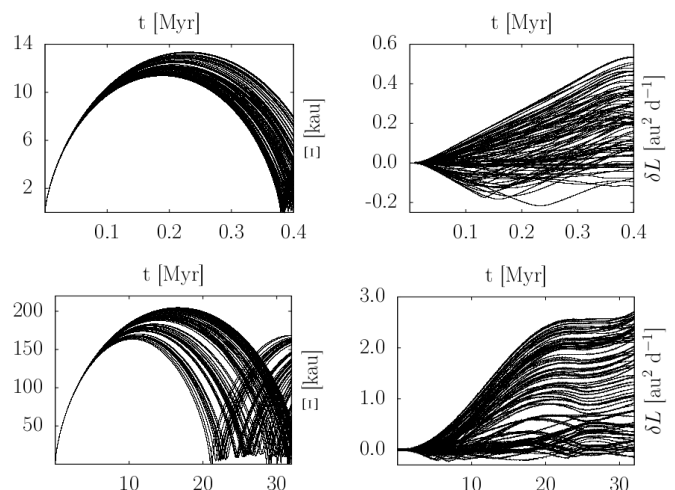


Fig. 13. Same as in Fig. 9 but now the particles were initialised with $a = 100$ kau. The top row represents an output of the Milgromian simulation, the bottom row of the Newtonian simulation. In MD simulation the follow up time, T_{rev} , is set to 0.4 Myr (see top left quarter of this figure for motivation), in Newtonian simulation T_{rev} is set to be the Keplerian period $T_{Kep}(a=100 \text{ kau}) \approx 32$ Myr.

correction to the Newtonian potential in the planetary region. They concluded the following constraints (on n):

$$v_n(\beta) = \left[\frac{1 + (1 + 4\beta^{-n})^{1/2}}{2} \right]^{1/n}, \quad n \geq 7, \quad (29a)$$

$$\widehat{v}_n(\beta) = [1 - \exp(-\beta^{-n/2})]^{-1/n}, \quad n \geq 6, \quad (29b)$$

$$\bar{v}_n(\beta) = [\widehat{v}_{2n}(\beta)] + \left(1 - \frac{1}{2n}\right) \exp(-\beta^n), \quad n \geq 2, \quad (29c)$$

where Eqs. (29a) - (29c) are three different families of the interpolating function v . Note that $\widehat{v}_1 = \bar{v}_{1/2}$. So far we have used only $\bar{v}_{1/2}$ in our calculations. But according to the findings of H+16 this interpolating function, although very popular, is ruled out. H+16 also revised the value of a_0 based on rotation curve fits (taking care whether EFE plays a role) and found optimum (best-fit) value for a given interpolating function. For example $\bar{v}_{n \geq 2}$ yields $a_0 \lesssim 8.1 \times 10^{-11} \text{ m s}^{-2}$, where the boundary value is a bit smaller than the standard value $a_0 = 1.2 \times 10^{-10} \text{ m s}^{-2}$, but still well compatible with the baryonic Tully-Fisher or Faber-Jackson relation. In what follows we consider only the \bar{v}_n family.

Fig. 17 shows $\bar{v}_\alpha(\beta)$ for $1 \leq \beta \leq 3$ and three different alphas, $\alpha = 0.5, 1.5$ and 2.0 . The rightmost dashed vertical line

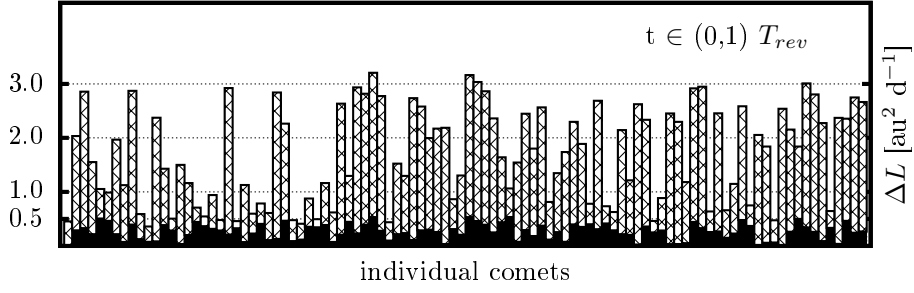


Fig. 14. Same as in Fig. 10 but now the particles were initialized with $a = 100$ kau. In MD simulation $T_{rev} = 0.4$ Myr, in Newtonian simulation $T_{rev} = T_{Kep}(a = 100 \text{ kau}) \approx 32$ Myr. A single bin corresponds to a single test particle in the simulation. Solid bins are ΔL in the simple model of the MOC, shaded bins, stacked on the solid bins, are ΔL in Newtonian dynamics with gravity of the Sun and the Galactic tide accounted.

marks the smallest possible β for the Solar System in the field of the Galaxy assuming $\bar{v}_{1.5}(\beta)$ and $a_0 = 8.1 \times 10^{-11} \text{ m s}^{-2}$. This was found by assuming the external field dominance and solving for g_e^N in $g_e - \bar{v}_{1.5}(g_e^N/a_0) g_e^N = 0$, what yields $\beta = 2.75$. If internal field is non-negligible then β is always larger. Note that $\bar{v}_{1.5}(2.75) \approx \bar{v}_{2.0}(2.75)$; as of this and numerical convenience of using $\bar{v}_{1.5}$ we consider combination $\bar{v}_{1.5}$ and $a_0 = 8.1 \times 10^{-11} \text{ m s}^{-2}$ in our calculations.

PMD, Eq. (20), as a function of heliocentric distance, Ξ , is depicted in Fig. 18 along ξ , η and ζ axes of $O_\odot(\xi, \eta, \zeta)$. The simple model of the MOC, $\bar{v}_{1.5}(\beta)$ interpolating function and $a_0 = 8.1 \times 10^{-11} \text{ m s}^{-2}$ were assumed. The peaks in the positive values of ρ_{ph} are ~ 800 (left one) and ~ 400 (right one) times smaller than in the case of $\bar{v}_{0.5}(\beta)$ and $a_0 = 1.2 \times 10^{-10} \text{ m s}^{-2}$. Note that MD predicts existence of ‘regions’ with negative PMD in the Solar System imposed to the gravitational field of the Galaxy (Milgrom 1986a). This speciality of PMD makes MD theoretically observationally distinguishable from the DM hypothesis.

We can conclude that adopting $\bar{v}_\alpha(\beta)$ with $\alpha = 1.5$ or 2.0 and $a_0 = 8.1 \times 10^{-11} \text{ m s}^{-2}$ - or even larger α and smaller a_0 (H+16) - we can expect the MOC to be very much Newtonian as EFE in this case essentially suppresses Milgromian regime at any distance from the Sun. The MOC is then of comparable overall size, comets have similar binding energies and the Jupiter-Saturn barrier operates similarly as in Newtonian dynamics. Aphelia directions of observed dynamically new comets were shown to avoid Galactic latitudes, b_G , close to the polar caps and the Galactic equator (Delsemme 1987). This is conventionally considered to be a signature of the Galactic tide induced injection of the comets (Torbett 1986; Delsemme 1987). Note that in the case $\bar{v}_{0.5}(\beta)$ and $a_0 = 1.2 \times 10^{-10} \text{ m s}^{-2}$ the MOC was shown to be compact and weakly influenced by the Galactic tide, what hence also suggest that an interpolating function steeper in the transition regime should be favoured.¹⁸

Anyway, even when interpolating functions and a_0 in line with the Cassini data are applied some effects of MD can be still present. Torquing of cometary perihelia due to EFE at heliocentric distances where the Galactic tide is weak can be important. To illustrate and quantify this effect we have plotted ΔL for the

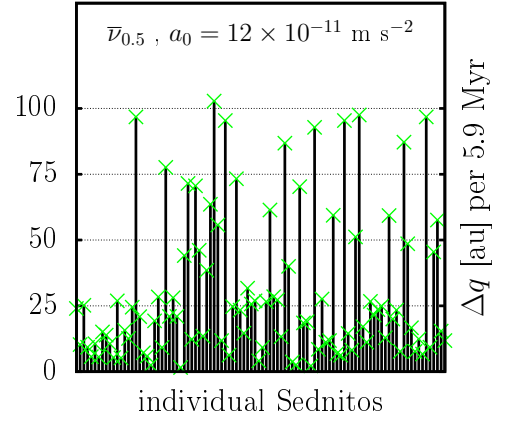


Fig. 15. $\Delta q \equiv q_{max} - q_{min}$ per 5.9 Myr for 100 Sedna progenitors (Sednitos) moving under the action of EFE. Sednitos were initialized at perihelia with $a = 524$ au, uniformly distributed $q \in (5, 30)$ au, $i \in (-10, 10)$ deg, ω and $\Omega \in (0, 2\pi)$.

same $a = 10$ kau Monte Carlo comets as in § 6.1 but now assuming QUMOND with $\bar{v}_{1.5}(\beta)$ and $a_0 = 8.1 \times 10^{-11} \text{ m s}^{-2}$ instead of $\bar{v}_{0.5}(\beta)$ and $a_0 = 1.2 \times 10^{-10} \text{ m s}^{-2}$. One revolution of a comet now corresponds well to Keplerian period as we are effectively in the Newtonian regime. We have used $\alpha = 1.5$, although H+16 found that α is constrained to be $\alpha \geq 2.0$, for its numerical convenience and to speed up our numerical calculations. Our aim is to see how effective is the torquing due to EFE when the whole MOC is essentially in the Newtonian regime, see Fig. 17, and in this sense $\alpha = 1.5$ with $a_0 = 8.1 \times 10^{-11} \text{ m s}^{-2}$ serve well.

Fig. 19 shows the value of $\Delta L \equiv L_{max} - L_{min}$ of the individual comets, where again $L_{max} \equiv [L(t)]_{max}$ and $L_{min} \equiv [L(t)]_{min}$ are the maximal and the minimal value of $L(t)$ during T_{rev} , assumed to be Keplerian period T_{Kep} as now $T_{rev} \approx T_{Kep}$. We can directly compare Figs. 10 and 19. In average ΔL is naturally smaller in the case of steeper interpolation function and smaller a_0 but extremal values in both cases are similar. This could explain why we are observing comets with relatively small semi-major axes, which should be prevented from being delivered into the inner Solar System due to the Jupiter-Saturn barrier (DK11), and in the same time, an imprint of the Galactic tide as inferred from the majority of observed comets.

7.1. Sedna

We are interested in how important is torquing of perihelion due to EFE in the trans-Neptunian region when one substitutes $\alpha = 0.5$ of $\bar{v}_\alpha(\beta)$ interpolating function and the standard value $a_0 =$

¹⁸ In Newtonian dynamics anisotropy in b_G of aphelia distribution is introduced due to existence of a distinguished direction, perpendicularly to the Galactic midplane. Considering the MOC with $\bar{v}_{0.5}(\beta)$ and $a_0 = 1.2 \times 10^{-10} \text{ m s}^{-2}$ - where injection of a comet due to tides is secondary - there is also a distinguished direction in the cloud, although varying with time, the direction of the external field of the Galaxy. Maybe the long term effect of the external field is to produce such anisotropy in b_G of aphelia distribution for MOC comets.

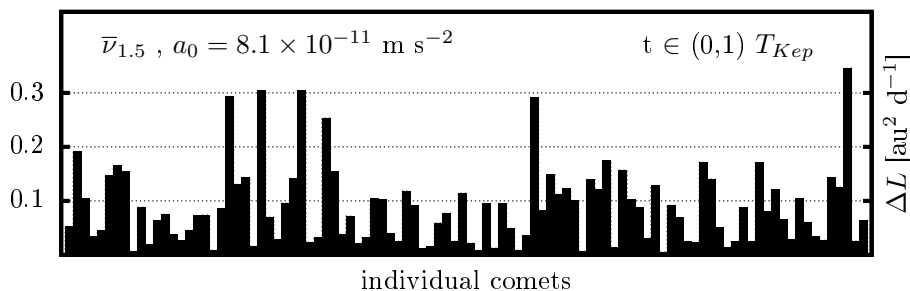


Fig. 19. Histogram of $\Delta L \equiv L_{max} - L_{min}$ for 100 Monte Carlo test particles initialised at perihelia with $a = 10$ kau and q uniformly distributed on the interval (15, 100) au and then evolved in the simple model of the MOC for $T_{rev} \approx T_{Kep} \approx 1$ Myr. $\bar{v}_{1.5}(\beta)$ and $a_0 = 8.1 \times 10^{-11} \text{ m s}^{-2}$ were used here instead of $\bar{v}_{0.5}(\beta)$ and $a_0 = 1.2 \times 10^{-10} \text{ m s}^{-2}$ as in Fig. 10. A single bin corresponds to a single test particle in the simulation.

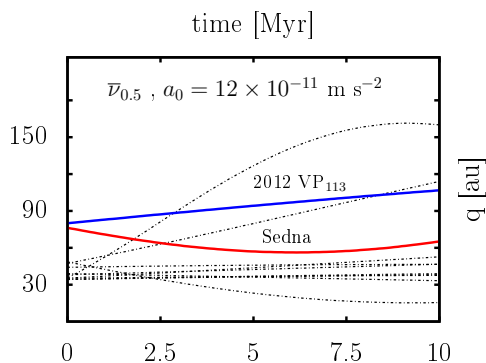


Fig. 16. Perihelion distance as a function of time under action of EFE for the known population of trans-Neptunian bodies with $a > 150$ au and $q > 30$ au. Thick solid lines are 2012 VP₁₁₃ and Sedna.

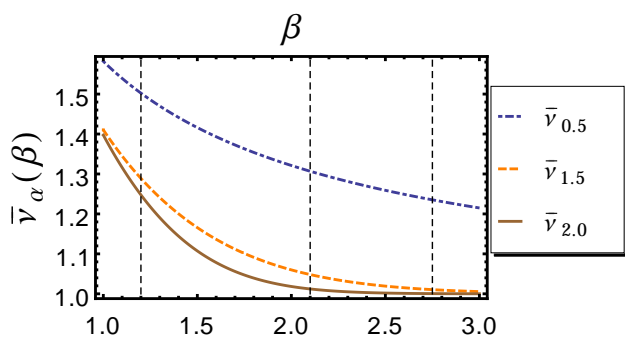


Fig. 17. Transition to the Newtonian regime for different alphas in \bar{v}_α family. Vertical dashed lines, from left to right, mark values $\beta \equiv g^N/a_0 = 1.20, 2.10$ and 2.75 , respectively. These came from $g_e - \bar{v}_\alpha(g_e^N/a_0) g_e^N = 0$, using $\alpha = 0.5, a_0 = 1.2 \times 10^{-10} \text{ m s}^{-2}$ ($\beta = 1.20$); $\alpha = 0.5, a_0 = 8.11 \times 10^{-11} \text{ m s}^{-2}$ ($\beta = 2.10$); $\alpha = 1.5, a_0 = 8.11 \times 10^{-11} \text{ m s}^{-2}$ ($\beta = 2.75$), and assuming that the external field dominates over the internal, $g^N \approx g_e^N$. When this is not the case the values of β are even larger. Note that $\bar{v}_{1.5}(2.75) \approx \bar{v}_{2.0}(2.75)$. g_e is always the same constant V_0^2/R_0 , but what matters is that the value of g_e varies in units of a_0 as one varies a_0 .

$1.2 \times 10^{-10} \text{ m s}^{-2}$ with larger values of α and $a_0 \leq 8.1 \times 10^{-11} \text{ m s}^{-2}$ (H+16).

We have run similar QUMOND simulation as in § 6.2 assuming $\bar{v}_{1.5}(\beta)$ and $a_0 = 8.1 \times 10^{-11} \text{ m s}^{-2}$. We have used the same initial orbit assignment for Sednitos as in § 6.2, except for

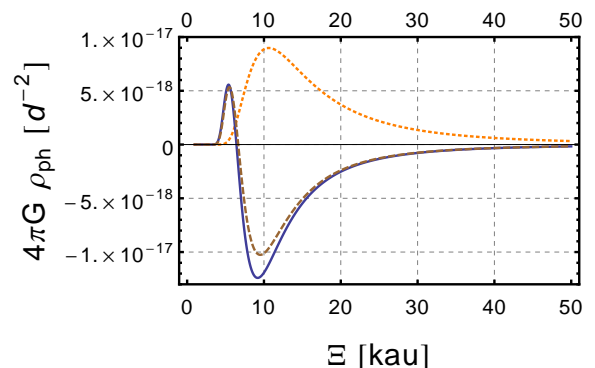


Fig. 18. PMD in the simple model of the MOC in the direction of ξ (solid line), η (dotted line) and ζ (dashed line) axis of $O_\odot(\xi, \eta, \zeta)$. $\bar{v}_{1.5}$ and $a_0 = 8.11 \times 10^{-11} \text{ m s}^{-2}$ are assumed.

the value of q which is now a random number uniformly distributed on the interval (25, 30) au, in order to maximise Δq . In Fig. 20 we show Δq per 10.0 Myr for 100 simulated Sednitos. The extremal Δq is about 50 au per 10.0 Myr. At the end of the simulation 2 Sednitos had $q \sim 75$ au, hence very close to the Sedna's perihelion distance. Sedna-like orbits (here simplified as specific a and q values) can be produced by EFE from those having protoplanetary-disk origin in ~ 10 Myr.

If interpolating function \bar{v}_α with $\alpha \geq 2.0$ would be used instead, then we can expect that larger times would be necessary to produce given Δq . We have tested this in approximation of the EFE induced quadrupole anomaly¹⁹ (Milgrom 2009b; Blanchet & Novak 2011) and quadrupole strengths listed in Hees et al. (2016). For \bar{v}_2 and $a_0 = 8.1 \times 10^{-11} \text{ m s}^{-2}$ the timescale of producing given Δq is in average by a factor of few larger.

In Fig. 21 we depict perihelion distance as a function of time, $q(t)$, for the known trans-Neptunian objects with $q > 30$ au and $a > 150$ au, in the next 10 Myr, assuming $\bar{v}_{1.5}(\beta)$ and $a_0 = 8.1 \times 10^{-11} \text{ m s}^{-2}$. None of the followed objects migrates under 30 au in the next 10 Myr.

8. Discussion and conclusion

We have investigated how does the (Newtonian) paradigm of a vast cometary reservoir, the Oort cloud (OC), change in Mil-

¹⁹ The inner OC can be crudely investigated with aid of the multipole expansion approach (Milgrom 2009b; Blanchet & Novak 2011), taking into account only the dominant quadrupole term and assuming constancy of the parameter Q_2 (Blanchet & Novak 2011; Hees et al. 2016). Rotation of the external field can be in this case easily build in.

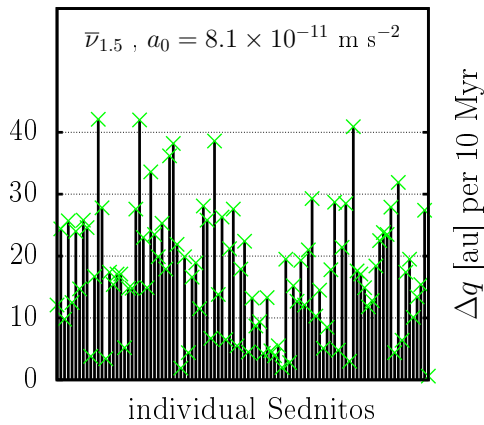


Fig. 20. $\Delta q \equiv q_{max} - q_{min}$ per 10.0 Myr for 100 Sedna progenitors (Sednitos) moving under the action of EFE. $\bar{v}_{1.5}(\beta)$ and $a_0 = 8.1 \times 10^{-11} \text{ m s}^{-2}$ were used instead of $\bar{v}_{0.5}(\beta)$ and $a_0 = 1.2 \times 10^{-10} \text{ m s}^{-2}$ as in Fig. 15. Sednitos were initialized at perihelia with $a = 524 \text{ au}$, uniformly distributed $q \in (25, 30) \text{ au}$, $i \in (-10, 10) \text{ deg}$, ω and $\Omega \in (0, 2\pi)$.

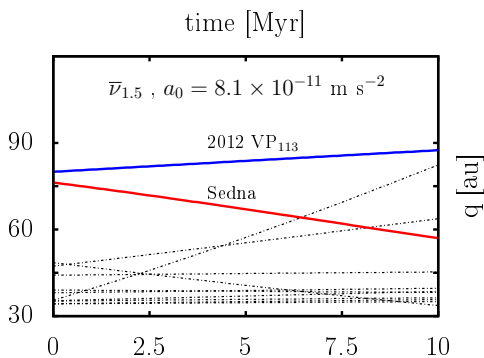


Fig. 21. Perihelion distance as a function of time under action of EFE for the known population of trans-Neptunian bodies with $a > 150 \text{ au}$ and $q > 30 \text{ au}$. $\bar{v}_{1.5}(\beta)$ and $a_0 = 8.1 \times 10^{-11} \text{ m s}^{-2}$ were used instead of $\bar{v}_{0.5}(\beta)$ and $a_0 = 1.2 \times 10^{-10} \text{ m s}^{-2}$ as in Fig. 16. Thick solid lines are 2012 VP₁₁₃ and Sedna.

gromian dynamics (MD), specifically in the modified gravity QUMOND. The results are dependent on the choice of the MD interpolating function and value of the constant a_0 .

For the popular pair, $\bar{v}_{0.5}$ [Eq. (29c) with $\alpha = 0.5$] and $a_0 = 1.2 \times 10^{-10} \text{ m s}^{-2}$, we have found the following qualitative properties of the Milgromian OC (MOC):

- The observationally inferred cloud is compact with radius $\sim 15 \text{ kau}$.
- Binding energies of comets are significantly increased compared to those of the classical OC. The planetary barrier shifts significantly inward.
- Injection of comets into the inner Solar System is mainly driven by the external field effect (EFE) due to the Galaxy, the specific feature of nonlinear MD, see § 2.3. The Galactic tide can be due to small heliocentric distances of MOC bodies neglected.
- EFE induced injection of the comets is very efficient and the cometary influx can be significantly larger than in the Newtonian case, assuming as 0. approximation the same, Newtonian, source population and its distribution in both frameworks.
- Orbit of a body with proto-planetary disk origin can be under action of EFE transformed to Sedna-like orbit on timescale of several Myr.

Trans-Neptunian bodies in Sedna-like orbits are not ‘fossil’ objects with frozen perihelia (like in the Sun-in-a-cluster model) but rather they could repeatedly migrate through the inner Solar System as EFE raises and lowers their perihelia repeatedly.

During the preparation of this paper H+16 published constraints on various commonly used MD interpolating function families. The constraints were based on the Cassini spacecraft radio tracking data (Hees et al. 2014). Many popular MD interpolating functions have been proven incompatible with the data, among which also $\bar{v}_{0.5}$. Adopting $\bar{v}_\alpha(\beta)$ with $\alpha \gtrsim 1.5$ and $a_0 \leq 8.11 \times 10^{-11} \text{ m s}^{-2}$ in line with H+16, the MD-regime is essentially suppressed at any distance from the Sun due to EFE, see Fig. 17. The cloud is in this case very much Newtonian in its overall size, binding energies of comets and operation of the Jupiter-Saturn barrier. Anyway, even in this case EFE substantially torques orbits in the inner parts of the cloud, where the tidal force is weak, with potential to transform primordial orbits to Sedna-like orbits as was shown in the case $\alpha = 1.5$ and $a_0 = 8.11 \times 10^{-11} \text{ m s}^{-2}$ on the timescale of $\sim 10 \text{ Myr}$. Steeper interpolating functions implies larger timescales for such transformation.

To sum up, if the results presented in Hees et al. (2014) are correct and there is no other hidden dynamical effect acting on the spacecraft then the results presented in §§ 4 - 6 are only of academical character. Still it is instructive to see how the MOC changes with varying description of the transition regime.

We further discuss the MOC in line of the new constraints on the MD interpolating function. We stress that the influence of EFE on inner OC bodies and Centaurs, Kuiper belt objects and scattered disk objects in high- a orbits is even under these circumstances substantial. Consequently Sedna-like orbits and orbits of large semi-major axis Centaurs are easily comprehensible in MD. In MD they both belong to the same population, just in different modes of their evolution.

MD could eventually shed light on many open problems in the cis and trans-Neptunian region. Besides the already mentioned puzzling orbits of Sedna and 2012 VP₁₁₃, the clustering in argument of perihelion, ω , near $\omega \approx 0 \text{ deg}$, for bodies in orbits with $q > 30 \text{ au}$ and $a > 150 \text{ au}$ (Trujillo & Sheppard 2014), and origin of high- a -Centaurs (Gomes et al. 2015), could be elucidated in MD. Concerning ω -clustering, EFE would manifest in this region through anomalous force increasing with heliocentric distance and aligned with the direction to the Galactic center (Milgrom 2009b; Blanchet & Novak 2011). Hence bodies protected from encountering the planets frequently should bear an imprint of EFE, similarly as if there was a distant massive body hidden deep in the OC. Although in MD one would rather expect clustering in the longitude of perihelion $\varpi = \omega + \Omega$ for low inclination orbits, or in general, the clustering in the physical space (Paučo 2016, in preparation). That subsample of the stable objects is actually clustered in the physical space was recently shown in Batygin & Brown (2016).

EFE is important dynamical agent, raising and lowering perihelia in the inner parts of the outer Solar System very effectively, with no such counterpart in the Newtonian dynamics. Thus, we could intuitively expect MOC, and especially its inner part, to be more populous at formation phase than the classical OC, as planetesimals with mildly pumped semi-major axes ($a \sim 0.1 - 1 \text{ kau}$) could have their perihelia lifted sufficiently rapidly to be protected from being ejected or captured by the planets. Also we could expect this primordial outward migration being followed by a period of high influx of interplanetary material, after which (or after several such cycles) was this inner region radically depleted. Here timing is important because this phenomenon could

coincide with the late heavy bombardment, hinted by the Moon petrology record (Hartmann et al. 2000), at ~ 700 Myr after the planets formed. Although such event is rather abrupt and of relatively short duration, what was well accounted in the Newtonian framework with the model of rapid migration of the outer planets (Gomes et al. 2005). We plan to investigate this topic in the subsequent work.

It is questionable whether the primordial disk mass and Oort-Scattered-Disk population ratio problems arise in the context of MD as nobody ever simulated Solar System formation and evolution (with its outermost parts) in MD. EFE torquing is important in the context of the (re)distribution of material within the cloud, which could be then expected to be different in MD than in the Newtonian dynamics. The preference of high semi-major axis orbits (where tides are sufficiently strong) in the classical OC does not need to be so eminent in MOC. In the perihelion distance, q , vs. semi-major axis, a , diagram, where in the classical OC theory there is more or less empty space at $q \gtrsim 100$ au, $a \sim 1000$ au, we expect some ‘residual’ population in MD. This could be in the future tested against observations. For example, a simulation similar to that in §§ 6.2 and 7.1, but including the outer planets and more Sednitos, would yield after some time steady populations of bodies with $q > 30$ au and $q < 30$ au (high- a Centaurs), what could be tested against observations on the similar grounds as in Gomes et al. (2015). There is obviously some tension between the theory and observations in the Newtonian framework (Gomes et al. 2015).

We cannot claim MD to be self-consistent solution of the puzzles bothering classical OC theory at this stage, but it was shown that it can well form new, testable, paradigm with specific signature in the outer parts of the Solar System.

Acknowledgements. We are thankful to Leonard Kornoš and Luboš Neslušan for valuable discussions on orbital integrators and the classical Oort cloud. We also thank the referee, Rodney Gomes, for an open-minded review and comments which help to improve the clarity of the paper and also inspired us to realize additional motivation for Milgromian dynamics in the Solar System. J.K. is supported by the Slovak National Grant Agency VEGA, grant No. 1/067/13.

References

- Angus, G. W., Gentile, G., Diaferio, A., Famaey, B., & van der Heyden, K. J. 2014, *MNRAS*, 440, 746
- Batygin, K. & Brown, M. E. 2016, *AJ*, 151, 22
- Begeman, K. G., Broeils, A. H., & Sanders, R. H. 1991, *MNRAS*, 249, 523
- Bekenstein, J. & Milgrom, M. 1984, *ApJ*, 286, 7
- Bekenstein, J. D. 2004, *Phys. Rev. D*, 70, 083509
- Berezhiani, L. & Khoury, J. 2015a, *ArXiv e-prints* [arXiv:1506.07877]
- Berezhiani, L. & Khoury, J. 2015b, *Phys. Rev. D*, 92, 103510
- Bienaymé, O., Famaey, B., Wu, X., Zhao, H. S., & Aubert, D. 2009, *A&A*, 500, 801
- Blanchet, L. & Bernard, L. 2014, *International Journal of Modern Physics Conference Series*, 30, 60271
- Blanchet, L. & Le Tiec, A. 2008, *Phys. Rev. D*, 78, 024031
- Blanchet, L. & Le Tiec, A. 2009, *Phys. Rev. D*, 80, 023524
- Blanchet, L. & Novak, J. 2011, *MNRAS*, 412, 2530
- Boylan-Kolchin, M., Springel, V., White, S. D. M., & Jenkins, A. 2010, *MNRAS*, 406, 896
- Brada, R. & Milgrom, M. 1995, *MNRAS*, 276, 453
- Brasser, R., Duncan, M. J., & Levison, H. F. 2007, *Icarus*, 191, 413
- Brasser, R. & Morbidelli, A. 2013, *Icarus*, 225, 40
- Brown, M. E., Trujillo, C., & Rabinowitz, D. 2004, *ApJ*, 617, 645
- Chambers, J. E. 1999, *MNRAS*, 304, 793
- Copeland, E. J., Sami, M., & Tsujikawa, S. 2006, *International Journal of Modern Physics D*, 15, 1753
- Delsemme, A. H. 1987, *A&A*, 187, 913
- Dones, L., Weissman, P. R., Levison, H. F., & Duncan, M. J. 2004, *Oort cloud formation and dynamics*, in *Comets II*, ed. M. C. Festou, H. U. Keller, & H. A. Weaver, 153–174
- Duncan, M., Quinn, T., & Tremaine, S. 1987, *AJ*, 94, 1330
- Duncan, M. J. & Levison, H. F. 1997, *Science*, 276, 1670
- Dybczyński, P. A. & Królikowska, M. 2011, *MNRAS*, 416, 51
- Dybczyński, P. A. & Królikowska, M. 2015, *MNRAS*, 448, 588
- Einstein, A. 1915, *Sitzungsberichte der Königlich Preußischen Akademie der Wissenschaften (Berlin)*, Seite 844–847
- Everhart, E. 1985, in *Dynamics of Comets: Their Origin and Evolution*, Proceedings of IAU Colloq. 83, held in Rome, Italy, June 11–15, 1984. Edited by Andrea Carusi and Giovanni B. Valsecchi. Dordrecht: Reidel, Astrophysics and Space Science Library. Volume 115, 1985, p.185, ed. A. Carusi & G. B. Valsecchi, 185
- Faber, S. M. & Jackson, R. E. 1976, *ApJ*, 204, 668
- Famaey, B. & Binney, J. 2005, *MNRAS*, 363, 603
- Famaey, B., Bruneton, J.-P., & Zhao, H. 2007, *MNRAS*, 377, L79
- Famaey, B. & McGaugh, S. 2013, *Journal of Physics Conference Series*, 437, 012001
- Famaey, B. & McGaugh, S. S. 2012, *Living Reviews in Relativity*, 15, 10
- Fernández, J. A. & Brunini, A. 2000, *Icarus*, 145, 580
- Gentile, G., Famaey, B., & de Blok, W. J. G. 2011, *A&A*, 527, A76
- Gomes, R., Levison, H. F., Tsiganis, K., & Morbidelli, A. 2005, *Nature*, 435, 466
- Gomes, R. S., Soares, J. S., & Brasser, R. 2015, *Icarus*, 258, 37
- Hartmann, W. K., Ryder, G., Dones, L., & Grinspoon, D. 2000, *The Time-Dependent Intense Bombardment of the Primordial Earth/Moon System*, ed. R. M. Canup, K. Righter, & et al., 493–512
- Hees, A., Famaey, B., Angus, G. W., & Gentile, G. 2016, *MNRAS*, 455, 449
- Hees, A., Folkner, W. M., Jacobson, R. A., & Park, R. S. 2014, *Phys. Rev. D*, 89, 102002
- Heisler, J. & Tremaine, S. 1986, *Icarus*, 65, 13
- Hills, J. G. 1981, *AJ*, 86, 1730
- Hogg, D. W., Quinlan, G. D., & Tremaine, S. 1991, *AJ*, 101, 2274
- Holmberg, J. & Flynn, C. 2004, *MNRAS*, 352, 440
- Ibata, N. G., Ibata, R. A., Famaey, B., & Lewis, G. F. 2014, *Nature*, 511, 563
- Ibata, R. A., Famaey, B., Lewis, G. F., Ibata, N. G., & Martin, N. 2015, *ApJ*, 805, 67
- Ibata, R. A., Lewis, G. F., Conn, A. R., et al. 2013, *Nature*, 493, 62
- Iorio, L. 2010a, *The Open Astronomy Journal*, 3, 156
- Iorio, L. 2010b, *The Open Astronomy Journal*, 3, 1
- Kaib, N. A. & Quinn, T. 2008, *Icarus*, 197, 221
- Kaib, N. A. & Quinn, T. 2009, *Science*, 325, 1234
- Kaib, N. A., Roškar, R., & Quinn, T. 2011, *Icarus*, 215, 491
- Khoury, J. 2015, *Phys. Rev. D*, 91, 024022
- Koda, J., Yagi, M., Yamanoi, H., & Komiyama, Y. 2015, *ApJ*, 807, L2
- Królikowska, M. 2014, *A&A*, 567, A126
- Kroupa, P. 2012, *PASA*, 29, 395
- Kroupa, P., Famaey, B., de Boer, K. S., et al. 2010, *A&A*, 523, A32
- Lada, C. J. & Lada, E. A. 2003, *ARA&A*, 41, 57
- Levison, H. F., Dones, L., & Duncan, M. J. 2001, *AJ*, 121, 2253
- Levison, H. F., Morbidelli, A., Vokrouhlický, D., & Bottke, W. F. 2008, *AJ*, 136, 1079
- Lüghausen, F., Famaey, B., & Kroupa, P. 2014, *MNRAS*, 441, 2497
- Lüghausen, F., Famaey, B., & Kroupa, P. 2015, *Canadian Journal of Physics*, 93, 232
- Lüghausen, F., Famaey, B., Kroupa, P., et al. 2013, *MNRAS*, 432, 2846
- McGaugh, S. S. 2004, *ApJ*, 609, 652
- McGaugh, S. S. 2005a, *Physical Review Letters*, 95, 171302
- McGaugh, S. S. 2005b, *ApJ*, 632, 859
- McGaugh, S. S. 2008, *ApJ*, 683, 137
- McGaugh, S. S., Schombert, J. M., Bothun, G. D., & de Blok, W. J. G. 2000, *ApJ*, 533, L99
- Milgrom, M. 1983a, *ApJ*, 270, 371
- Milgrom, M. 1983b, *ApJ*, 270, 365
- Milgrom, M. 1986a, *ApJ*, 306, 9
- Milgrom, M. 1986b, *ApJ*, 302, 617
- Milgrom, M. 1994, *Annals of Physics*, 229, 384
- Milgrom, M. 1999, *Physics Letters A*, 253, 273
- Milgrom, M. 2001, *MNRAS*, 326, 1261
- Milgrom, M. 2009a, *Phys. Rev. D*, 80, 123536
- Milgrom, M. 2009b, *MNRAS*, 399, 474
- Milgrom, M. 2009c, *ApJ*, 698, 1630
- Milgrom, M. 2010, *MNRAS*, 403, 886
- Milgrom, M. 2011, *Acta Physica Polonica B*, 42, 2175
- Milgrom, M. 2015, *MNRAS*, 454, 3810
- Morbidelli, A. & Levison, H. F. 2004, *AJ*, 128, 2564
- Morbidelli, A., Tsiganis, K., Crida, A., Levison, H. F., & Gomes, R. 2007, *AJ*, 134, 1790
- Navarro, J. F., Frenk, C. S., & White, S. D. M. 1997, *ApJ*, 490, 493
- Neslušan, L. & Jakubík, M. 2013, *Contributions of the Astronomical Observatory Skalnaté Pleso*, 43, 109
- Oort, J. H. 1950, *Bull. Astron. Inst. Netherlands*, 11, 91
- Öpik, J. H. 1932, *Proc. Amer. Acad. Art and Sc.*, 67, 169
- Pawlowski, M. S., Famaey, B., Jerjen, H., et al. 2014, *MNRAS*, 442, 2362

Table 1. Original barycentric orbital elements of § 5 near-parabolic comets. These 31 comets were identified as dynamically new (assuming Newtonian dynamics) in the sample of DK11. Presented orbital elements are expected values retrieved from Królikowska (2014), errors are omitted. Successive columns are: comet designation, osculation date, perihelion distance, eccentricity, inclination, argument of perihelion, longitude of ascending node (all angles in equinox J2000.0), semi-major axis and perihelion passage time.

Comet	Epoch	q^\dagger	e	i^\dagger	ω^\dagger	Ω^\dagger	a^\dagger	T^\ddagger
[...]	[yyyymmdd]	[au]	[...]	[deg]	[deg]	[deg]	[kau]	[yyyymmdd]
C/1974 V1	16670721	6.02	0.99989464	60.9	151.8	226.1	57.110	19740808
C/1978 A1	16701212	5.61	0.99978957	116.9	343.4	211.7	26.652	19770722
C/1978 G2	16710809	6.28	1.00014083	153.2	229.7	72.2	-44.603	19780826
C/1984 W2 [◊]	16820212	4.00	0.99991890	89.3	255.3	250.2	49.383	19850929
C/1987 W3	16850706	3.32	0.99991866	76.8	195.1	198.4	40.850	19880119
C/1988 B1	16811015	5.03	0.99989942	80.6	124.2	325.2	50.025	19870319
C/1992 J1	16910824	3.00	0.99991839	124.3	83.5	203.3	36.765	19930904
C/1997 A1	16950405	3.16	0.99993098	145.1	40.0	135.7	45.830	19970620
C/1997 BA6 [◊]	16970213	3.44	0.99989050	72.6	285.9	317.7	31.417	19991128
C/1999 J2	16910317	7.11	0.99984298	86.4	127.1	50.1	45.310	20000405
C/1999 K5	16980208	3.25	0.99993034	89.5	241.5	106.3	46.707	20000703
C/1999 U4	16960618	4.89	0.99984462	52.1	77.8	32.4	31.447	20011029
C/2000 A1	16861029	9.74	0.99960423	24.6	14.3	111.9	24.612	20000715
C/2001 C1	16960906	5.11	0.99991858	68.9	220.0	33.8	62.775	20020328
C/2001 K3	16990214	3.07	0.99990440	52.0	3.4	289.8	32.103	20010423
C/2001 K5	16970325	5.19	0.99994997	72.5	47.1	237.5	103.734	20021011
C/2002 A3	16960906	5.14	0.99989342	48.1	329.6	136.7	48.263	20020425
C/2002 J4	17000817	3.64	0.99987674	46.5	230.7	70.9	29.516	20031003
C/2002 L9	16950224	7.04	0.99974285	68.4	231.4	110.5	27.360	20040405
C/2003 G1	16971120	4.92	0.99993277	66.8	11.5	246.1	73.206	20030204
C/2003 S3	16920530	8.13	0.99971781	151.5	154.4	226.3	28.802	20030409
C/2004 P1	16960509	6.02	0.99981290	28.8	16.5	284.2	32.185	20030809
C/2004 T3	16901227	8.87	0.99959502	71.9	259.7	50.4	21.891	20030414
C/2004 X3	17010414	4.39	0.99994104	81.2	202.4	343.0	74.460	20050618
C/2005 B1 [◊]	17040109	3.21	0.99998720	92.5	103.1	195.6	250.627	20060222
C/2005 G1	17001215	4.95	0.99991785	108.4	113.9	299.6	60.314	20060226
C/2005 K1 [◊]	17021205	3.69	0.99996944	77.8	135.0	106.3	120.773	20051121
C/2005 Q1	16971120	6.40	0.99985473	105.3	44.8	87.7	44.053	20050826
C/2006 E1	16991001	6.04	0.99980395	83.2	232.8	95.1	30.788	20070106
C/2006 K1	17030404	4.42	0.99992817	53.9	296.5	72.2	61.576	20070720
C/2007 Y1	17050722	3.34	0.99988596	110.1	357.1	133.1	29.317	20080318

Notes. ^(◊) Non-gravitational effects are accounted in the orbit determination, see DK11. ^(†) These orbital elements are rounded from those of Królikowska (2014). ^(‡) .ddddd part is omitted compared to Królikowska (2014).

- Pawłowski, M. S., Famaey, B., Merritt, D., & Kroupa, P. 2015, ApJ, 815, 19
Pawłowski, M. S., Kroupa, P., Angus, G., et al. 2012a, MNRAS, 424, 80
Pawłowski, M. S., Kroupa, P., & Jerjen, H. 2013, MNRAS, 435, 1928
Pawłowski, M. S., Pflamm-Altenburg, J., & Kroupa, P. 2012b, MNRAS, 423, 1109
Rickman, H. 2014, Meteoritics and Planetary Science, 49, 8
Rickman, H., Fouchard, M., Froeschlé, C., & Valsecchi, G. B. 2008, Celestial Mechanics and Dynamical Astronomy, 102, 111
Sanders, R. H. 2003, MNRAS, 342, 901
Sanders, R. H. 2005, MNRAS, 363, 459
Sanders, R. H. 2010, MNRAS, 407, 1128
Schönrich, R. 2012, MNRAS, 427, 274
Sellwood, J. A. & Binney, J. J. 2002, MNRAS, 336, 785
Serenio, M. & Jetzer, P. 2006, MNRAS, 371, 626
Torbett, M. V. 1986, MNRAS, 223, 885
Trujillo, C. A. & Sheppard, S. S. 2014, Nature, 507, 471
Tully, R. B. & Fisher, J. R. 1977, A&A, 54, 661
Wu, X., Famaey, B., Gentile, G., Perets, H., & Zhao, H. 2008, MNRAS, 386, 2199
Wu, X., Zhao, H., Famaey, B., et al. 2007, ApJ, 665, L101
Zhao, H. & Famaey, B. 2010, Phys. Rev. D, 81, 087304
Zhao, H. & Famaey, B. 2012, Phys. Rev. D, 86, 067301
Zhao, H., Famaey, B., Lüghausen, F., & Kroupa, P. 2013, A&A, 557, L3
Złosnik, T. G., Ferreira, P. G., & Starkman, G. D. 2007, Phys. Rev. D, 75, 044017